Centre de recherche sur l'environnement alpin
Zentrum für alpine Umweltforschung
Research center on alpine environment

Master Project:

Assimilation of snow depth data from Sentinel-1 to improve the hydrological model of the Borgne catchment (VS)

March 11, 2021

Handed in by: Max Hurni
Supervisor: Dr. Giovanni De Cesare, EPFL
In-company supervisor: Dr. Tristan Brauchli, Crealp
External expert: Khalid Essyad, BG Ingénieurs

Abstract

Since 2013, Crealp (**C**entre de **R**echerche sur l'**E**nvironnement **A**lpin) is operating a real-time flood forecasting system for the upper Rhone river basin. The scarcity of meteorological input data at high elevation leads to model uncertainties. In this project, possible improvements of the sub-model of the Borgne catchment were tested and compared to the operational model and a newly calibrated model using the discharge measurement of the Grande Dixence network. First, a new snowmelt model considering measured solar radiation was tested. Second, the Sentinel-1 derived snow depth product by Lievens et al. (2019) was assimilated in the hydrological model during three winters between 2017 and 2019. The integration of solar radiation showed a promising increase of performance, especially for high elevation catchments. The assimilation of snow data led to contrasting results: some configurations showing a good improvement and some others are less convincing. The differences between modelled and measured water volumes and the validation with MODIS snow cover data led to the conclusion that non-assimilated models underestimate the snowpack, while the assimilated models tend to an overestimation. In the end, some ideas for subsequent steps are given in the outlook.

Résumé

Depuis 2013, le Crealp (**C**entre de **R**echerche sur l'**E**nvironnement **A**lpin) exploite un système de prévision des crues en temps réel pour le bassin versant du Rhône alpin. La disponibilité limitée de données météorologiques à haute altitude engendre des incertitudes dans la modélisation. Dans ce projet, des améliorations possibles du sous-modèle du bassin versant de la Borgne ont été testées et comparées au modèle opérationnel et à un modèle nouvellement calibré utilisant les mesures de débit du réseau de la Grande Dixence. Premièrement, un nouveau modèle de fonte des neiges qui tient compte du rayonnement solaire mesuré a été utilisé. Ensuite, le produit d'épaisseur de neige dérivé de Sentinel-1 par Lievens et al. (2019) a été assimilé dans le modèle hydrologique au cours des trois hivers entre 2017 et 2019. L'intégration du rayonnement solaire a montré une amélioration prometteuse des performances, en particulier pour les bassins versants en altitude. L'assimilation des données de neige a conduit à des résultats contrastés: certaines configurations montrent une amélioration alors que pour d'autres, les résultats sont moins convaincants. Les différences entre les volumes d'eau modélisés et mesurés et la validation avec les données MODIS sur la couverture neigeuse ont conduit à la conclusion que les modèles non-assimilés sous-estiment le manteau neigeux, alors que les modèles assimilés tendent à une surestimation. Pour finir, quelques idées d'amélioration pour le futur sont données dans les conclusions.

Acknowledgements

I would like to thank Dr. Giovanni De Cesare from EPFL ENAC LCH for the supervision of this master project. This project was realised in colaboration with the Centre de recherche sur l'environnement alpin (Crealp) in Sion. I would like to thank the director, Dr. Antonio Abellan, for this opportunity and his support. Merci also to Dr. Bastien Roquier and Dr. Javier Fluxia for the various hints and answers. Special thanks to Dr. Tristan Brauchli, who mentored my work. He contributed considerably to the development of this work and supported me in all stages. I always found the collaboration constructive and encouraging. Merci beaucoup also for proofreading this report. A thank you goes out to Crealp for providing me a computer and a workstation. I would also like to thank the various other crealp employees whom I had the opportunity to get to know during the project.

For this project, various data were obtained from different providers. I would like to thank Michel Bovey from SLF for the permission to use IMIS snow data and Adrien Michel from CRYOS at EPFL for providing it. I would like to thank Christian Constantin and Mike Imboden from HYDRO Exploitation SA. They not only provided me with the snow data from Stafel and the discharge data from numerous intakes in the Grande Dixence region, but also answered so many of my questions. I would also like to thank Yves Pigueron from FMV SA for providing the discharge data of the turbine of Bramois. Many thanks to Dr. Hans Lievens for the information on the Sentinel-1 product and to Dr. Tobias Jonas for providing the Matlab code to convert snow depth to snow water equivalent.

The work was carried out in autumn 2020 and winter 2021 during the Covid 19 pandemic. I was therefore forced to work from home for long periods of time. I would like to thank my flatmates for the co-working space in the warm kitchen. I would also like to thank my grandmother Coca and my parents Lisa and Pesche for the working space they generously made accessible to me. Plus, I would like to thank my cat, who occasionally tempted me to take a breather by feeding her. Finally, I would like to thank Rebecca for proofreading the report and for all the love and patience you gave me during the working process.

Contents

1. Introduction

Water paves the way for life. For humans just as much as for animals, plants and other organisms. On the blue planet, this resource is present everywhere: in oceans, in water bodies, in the soil and even in the air. Only about 2.5% of the global water volume is present as freshwater, of which about 75% is stored in glaciers or permanent snow cover [Shiklomanov (1993)]. More than one sixth of the world's population depends on water from glaciers and seasonal snowpack [Barnett et al. (2005)]. Besides its contribution to life, water can also lead to disastrous consequences. Too little water can cause extreme droughts, crop losses and starvation. On the other hand, too much water leads to flooding, land slides and thereby major damage to infrastructure and human lives. Nowadays, flood damage is responsible for one third of the costs induced by natural hazards worldwide [Bosello et al. (2018)].

During the last decades, Switzerland has experienced flooding on a regular basis: floods in Bern and other cities (Spring 1999 and 2004); major flood in the Canton of Valais (Fall 2000); century flood in Central Switzerland (2005) to name just a few examples. Over a hundred people died due to floods in Switzerland between 1946 and 2015 [Andres et al. (2017)]. Steep alpine catchments lead to rapid hydraulic responses during major rainfall events. Since many riverbeds have been straightened during the last century, their flow capacity decreased. This increased the risk of rivers bursting their banks. The consequences for towns and villages are often fatal. In the past years, measures such as the restoration of riverbeds and the creation of retention zones have therefore often been demanded and also implemented. In the Canton of Valais, which covers almost the entire upper Rhone river basin, the third Rhone correction is currently being carried out in a step-wise manner [CantonValais (2006)]. In addition to structural measures, reliable flood forecasting models have become an important pillar of flood protection [Adams & Pagano (2016)]. This allows, for example, the early lowering of water levels in regulated lakes in order to guarantee a reserve volume for the storage of flood peaks.

Since 2013, Crealp (**C**entre de **R**echerche sur l'**E**nvironnement **A**lpin) is operating a real-time flood forecasting system for the upper Rhone river basin based on weather forecasts. The aim is to provide a robust forecast for floods and, whenever possible, mitigate the impacts by better coordinating the operations of multiple hydropower plants located in the region. The project is called MINERVE (for **M**odélisation des **I**ntempéries de **N**ature **E**xtrême du **R**hône **V**alaisan et de leurs **E**ffets) and was first implemented by F. Jordan (2007). He used the Routing Systems II software to model hydrological processes in the Canton of Valais. The Canton of Valais has supported this project financially from the beginning. The MINERVE project was further developed by various authors [García Hernández (2011), García Hernández et al. (2014), Foehn et al. (2020)]. The most up-to-date software is now called RS MINERVE (for Routing System MINERVE) and is maintained and provided open source by Crealp [García Hernández et al. (2020), Foehn et al. (2019)]. The investigation of the model, mostly by comparing the modelled discharge with observations or the modelled snowcover with data from MODIS, allowed accurate insights into possible problems with snow modelling at high altitudes [Foehn et

al. (2020)]. Foehn has tried to improve the precipitation input data using a combination of data from weather stations and radar information. He discovered that this so called CombiPrecib-product [Sideris et al. (2014)] often underestimates snow depths at high elevation. Gugerli et al. (2020) found that CombiPrecip was underestimating the snow water equivalent (SWE) over glaciers by a factor between 2.2 and 3.7.

At high altitude, the collection of regular meteorological measurements such as snow depths and solid precipitation is more difficult because of harsh environmental conditions [Reist & Weingartner (2005)]. As a result, the level of coverage is lower. Various remote sensing techniques have already been successfully used to fill these data gaps. For example, Foehn et al. (2020) calibrated the RS MINERVE model using MODIS snow cover data. Vögeli et al. (2016) increased the performance of snow simulation significantly by using an airborne digital sensor (ADS) with a resolution of two meters. Baba et al. (2018) used Sentinel-2 observations of the snow cover to dynamically reduce the biases in temperature and precipitation data. And finally, Avanzi et al. (2020) has used snow course data to determine the deviation of the SWE in larger elevations. In the outlook of their studies, Avanzi and Baba suggested a possible use of Sentinel-1 snow data. According to Lievens et al. (2019), Sentinel-1 is the best suited SAR (Synthetic Aperture Radar) mission for snow monitoring. The revisit time of 6 days allows a near-real-time monitoring. In Lievens et al. (2019), they used a novel combination of co- and cross-polarised backscatter measurements to calculate snow depths in the Northern Hemisphere, with a resolution of 1 km^2. The magnitude of the Sentinel-1 snow depth retrievals was scaled by a parameter a. For its calibration, they used in situ measurements over the Northern Hemisphere mountain areas.

The aim of this work is to quantify the added-value of snow estimates from Sentinel-1 [Lievens et al. (2019)] for hydrological modelling. For this purpose, the remotely sensed snow depths were assimilated into the RS MINERVE model of the Borgne catchment in Valais. Foehn, who also used the RS MINERVE model in his thesis, suggested in his conclusions the integration of radiation data in the snow routine. In the present project, an attempt is made to improve the model by integrating the melt model from Pellicciotti et al. (2005), which includes incoming shortwave radiation and snow albedo.

1.1. Research questions

In the present project, one will answer the following research questions:

1. How accurate are the snow estimates from Sentinel-1 satellite [Lievens et al. (2019)] inside and near the Borgne catchment (VS)?
2. What is the performance of the operational and a newly calibrated RS MINERVE model of the Borgne river based on the following observations:
   a) discharges in Bramois and from the network of water intakes of Grand Dixance?
   b) snow depth estimates from Sentinel-1?
3. To what extent can the performance of the Borgne model be improved by:
   a) introducing a new model for snow and ice melt considering solar radiation and albedo?
   b) assimilating snow depth data from Sentinel-1 at peak of accumulation?

This report is divided in five chapters. The first chapter includes the introduction, the research questions and a description of the project perimeter. The following three chapters deal each with one of the above research questions. First, the snow depths derived from Sentinel-1 satellite are validated against local measurements collected inside and around the project perimeter. This allowes a better assessment of the advantages and limitations of this product for its further use. In the next chapter, the hydrological model is presented. The operational MINERVE model has been modified with newly available data and calibrated. The modelled snow depths are then compared with the ones from Sentinel-1. The fourth chapter focuses on the improvement of the model. On one hand, the snow and ice routines are modified by integrating measured shortwave radiation instead of the simple degree-day approach. On the other hand, the snow data derived from Sentinel-1 are assimilated into the model. Both models, as well as a combination of the two, are recalibrated and compared with each other. For this purpose, various performance indicators and a total of 10 comparison points with discharge measurements in the area are used. Finally, the snowcover extent is validated in spring using MODIS snow cover data. The last chapter contains the conclusions and presents some outlook.

1.2. Project perimeter

The project perimeter was the catchment area of the Borgne river in the Canton of Valais (Switzerland), as presented in Figure 1. It covers an area of 384 km^2, of which 55 km^2 are glaciers. The elevation change between the lowest and the highest point is remarkable: from the summit of the "Dent Blanche" (4357 masl) to the confluence of the Borgne into the Rhone (495 masl), there is a difference of 3862 metres. Figure 2 shows two impressions of the area. The main valley, the *Val d' Hérens*, splits in *Les Haudères* into the valley of *Arolla* and the valley of *Ferpècle*. The rivers in these valleys are accordingly called Borgne of Ferpècle and Borgne of Arolla. The most important confluence to the

Borgne is the Dixence, which originates in the *Val d'Hérémence* and joins the Borgne just downstream the village of *Hérémence*. The famous Grande Dixence dam is also located in this subvalley.

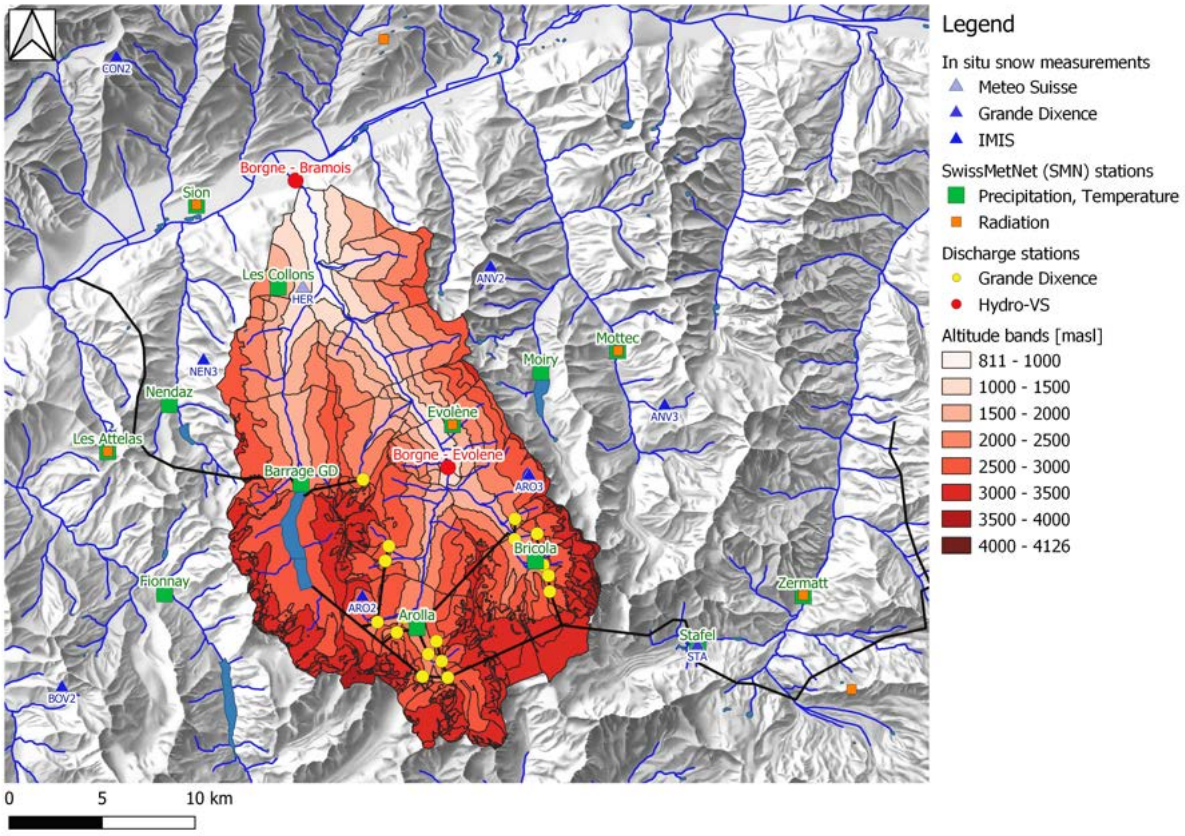

Figure 1: The catchment of the Borgne subdivited into altitude bands and the locations of different hydro-meteorological stations (background map: ©2004-2019 swisstopo).

In general, the flow regime of the Borgne is strongly influenced by hydropower. The supply network of the Grande Dixence reservoir has numerous water intakes distributed over the entire upper basin. The water is gathered in collection channels and routed underground to the reservoir. At a total of 17 points, the water is measured for monitoring purposes. These measurements, together with the discharge measurement in Bramois, near the confluence with the Rhone river, are essential for the evaluation of the hydrological model in this project. In Ferpècle and Arolla water is pumped towards the Grande Dixence reservoir. The turbines of this hydropower plant in *Bieudron* release the water directly into the Rhone and consequently out of the catchment area. Another hydropower plant is located in *Le Chomplong*. The water is released upstream of the discharge measurement point in *Bramois* and thus has a major influence on the hydrological regime. Fortunately, timeseries on both turbines of in *Bieudron* and *Bramois* are available for this project. However, the data for the two pumping stations were not available.

Figure 2: Impressions of the valley. Left: the view into the *Val d'Hérémence*, the Grande Dixence dam can be seen slightly in the back. Right: the renowned *pyramids of Euseigne* and the view out of the valley (Photos by M. Hurni).

2. Validation of Sentinel-1 data

2.1. Introduction

A recent study by Lievens et al. (2019) has proven the ability of the Sentinel-1 constellation to estimate snow depth in the Northern Hemisphere. They showed the potential of snow depth data derived from remote sensing at a high spatial resolution (1 km^2) using an empirical change detection approach.[1] They validate the product against ∼4000 sites in the whole Northern Hemisphere, obtaining an average Mean Absolute Error (MAE) of 0.18 m and a bias within ±0.1 m for most of the sites.
In addition to the original product, Lievens provides an improved version called Sentinel-1 "exp", that comes with less temporal smoothing. This is intended to ensure that the product is available in near real-time by reducing computational efforts. The "exp" product also promises to mask out wet snow conditions. Wet snow reflects the radar signal much better than fresh snow and is thereby the reason of a systematic underestimation of snow depth during the melting period. Lievens used a ratio of measurements in cross- and co-polarization to mitigate the impact of wet snow. Plus, he tries to detect drops in backscatter, which are caused by wet snow, and stop the retrieval after this detection. This wet snow detection was initiated after February.[2] For the sake of clarity, the product derived from the article is called "base", the upgraded product is called "exp" throughout this report.

Before the product is used for data assimilation in the Borgne catchment, it should be compared with snow measuring stations in and near the area of interest. In this chapter, the two products "base " and "exp" are compared with 10 in situ measuring stations. The observations are provided by different operators and are located between 1218 and 2847 meters above sea level (masl). This should also allow the choice of suitable dates which strike the peak of accumulation for snow assimilation.

2.2. Methodology

2.2.1. Sentinel-1

The two Sentinel-1 products "base" and "exp" were assessed separately. The evaluated time span for the "base" one stretches from 01.09.2016 to 15.05.2019 and for the "exp" one from 01.09.2016 to 08.04.2020, with a revisit time of six days. The original dataset was a raster with a spatial resolution of 1 km^2. To compare the products with in situ measurements, time series from the raster cells, in which in situ stations are located, were created using the packages *ncdf4*, *raster* and *maptools* from RStudio[3].

[1] Lievens's product is available open source on https://ees.kuleuven.be/project/c-snow

[2] Information about the "exp" product plus the product itself were received within an email conversation between H. Lievens and T. Brauchli (Crealp) in autumn 2020.

[3] R Studio version 1.2.1335; 'ncdf4' version 1.17; 'raster' version 3.3-13; 'maptools' version 1.0-2

2.2.2. Snow depth to SWE conversion

Sentinel-1 provides snow depth estimates. However, in the RS MINERVE software used later, the snow water equivalent (SWE) is calculated. SWE, indicated in metres, is the height of the water column that would result if the entire snowpack was melted. This parameter is thus independent of the snow density. Jonas et al. (2009) has developed an empirical model for converting a measured snow depth to SWE. For that, they analysed the data of snow depth and snow density of 37 measuring points throughout Switzerland. This allows the calculation of a bulk snow density as a function of season, snow depth, site altitude and location. They also provide a Matlab code that allows a straightforward conversion[1]. This model was used for the conversion of Sentinel-1 data whenever SWE was needed instead of snow depth.

2.2.3. In situ snow measurements

The ten considered stations are listed in Table 1 and also shown in Figure 1. Eight of them are from the IMIS-Network of the Institute for Snow and Avalanche Research [SLF (2020)]. The SwissMetNetwork (SMN) of MeteoSwiss (2020) and the GrandeDixenceSA (2020) each operate one of the remaining stations. For the station of Stafel, data cleansing was carried out as follows: zero values in winter were deleted; in summer, values below 5 cm were set to zero.

Table 1: List of in situ snow stations that were used in this project.

Name	Label	Operator	X coordinate	Y coordinate	Elevation [masl]
Anniviers Orzival	ANV2	IMIS	607468	115206	2640
Anniviers Traquit	ANV3	IMIS	616833	107764	2589
Arolla Breona	ARO3	IMIS	609546	103997	2602
Arolla Les Fontanesses	ARO2	IMIS	600558	97471	2847
Boveire	BOV2	IMIS	584389	92601	2687
Conthey	CON2	IMIS	587328	126494	2229
Heremence	HER	SMN	597356	114092	1218
Nendaz	NEN3	IMIS	592014	110194	2203
Stafel	STA	Dixence	618599	94893	2182
Vallee de la Sionne	VDS2	IMIS	594521	130015	2385

2.2.4. Performance indicators

In Lievens et al. (2019), they calculated the MAE and the bias for the evaluation (among others). In addition to these two indicators, the root mean squared error (RMSE) was calculated in this project. Calculations where done with Rstudios using the package *metrics*.[2] The three indicators are briefly explained hereafter.

[1] implementation by T. Jonas, SLF Switzerland, June 2012.

[2] RStudio: Version 1.2.1335; 'metrics': Version 0.1.4

MAE: the mean absolute error [m] computes the average absolute difference between two datasets using Eq. 1a.

BIAS: the bias [m] is the difference between the average of the Sentinel-1 data and the average of the in-situ values (Eq. 1b).

RMSE: the root mean squared error [m] is the standard deviation of the prediction errors according to Eq. 1c.

$$MAE = \frac{\sum_{i=1}^{n} |y_i - x_i|}{n} \tag{1a}$$

$$BIAS = \frac{\sum_{i=1}^{n} y_i}{n} - \frac{\sum_{i=1}^{n} x_i}{n} \tag{1b}$$

$$RMSE = \sqrt{\frac{\sum_{i=1}^{n} (y_i - x_i)^2}{n}} \tag{1c}$$

with y_i as the Sentinel-1 data and x_i the observed values from in situ stations. n is the number of observations.

2.3. Results

Figure 3 shows the comparison of in situ measurements and the Sentinel-1 "base" snow depth. In Figure 4, the "exp" product is compared with the same measurements. For both figures the associated indicators are given in the plots. The dynamics of snow accumulation until the peak are reasonably well reproduced for both products and for years with low snowfall (2017) and years with high snowfall (2018). However for some stations, the differences are large (for example HER, ANV3). The deviations during the melting period, which were already mentioned in Lievens's publication, are visible in the "base" product. These values are removed in the "exp" product.

The mean values of the indicators for the ten stations are given in Table 2. The RMSE and the MAE are better for the "exp" product. This is explained by the elimination of outliers in spring, which improves the performances.

Table 2: Mean indicators for the two Sentinel 1 products "base" and "exp".

	base	exp
RMSE	0.57	0.44
MAE	0.40	0.29
BIAS	-0.02	-0.03

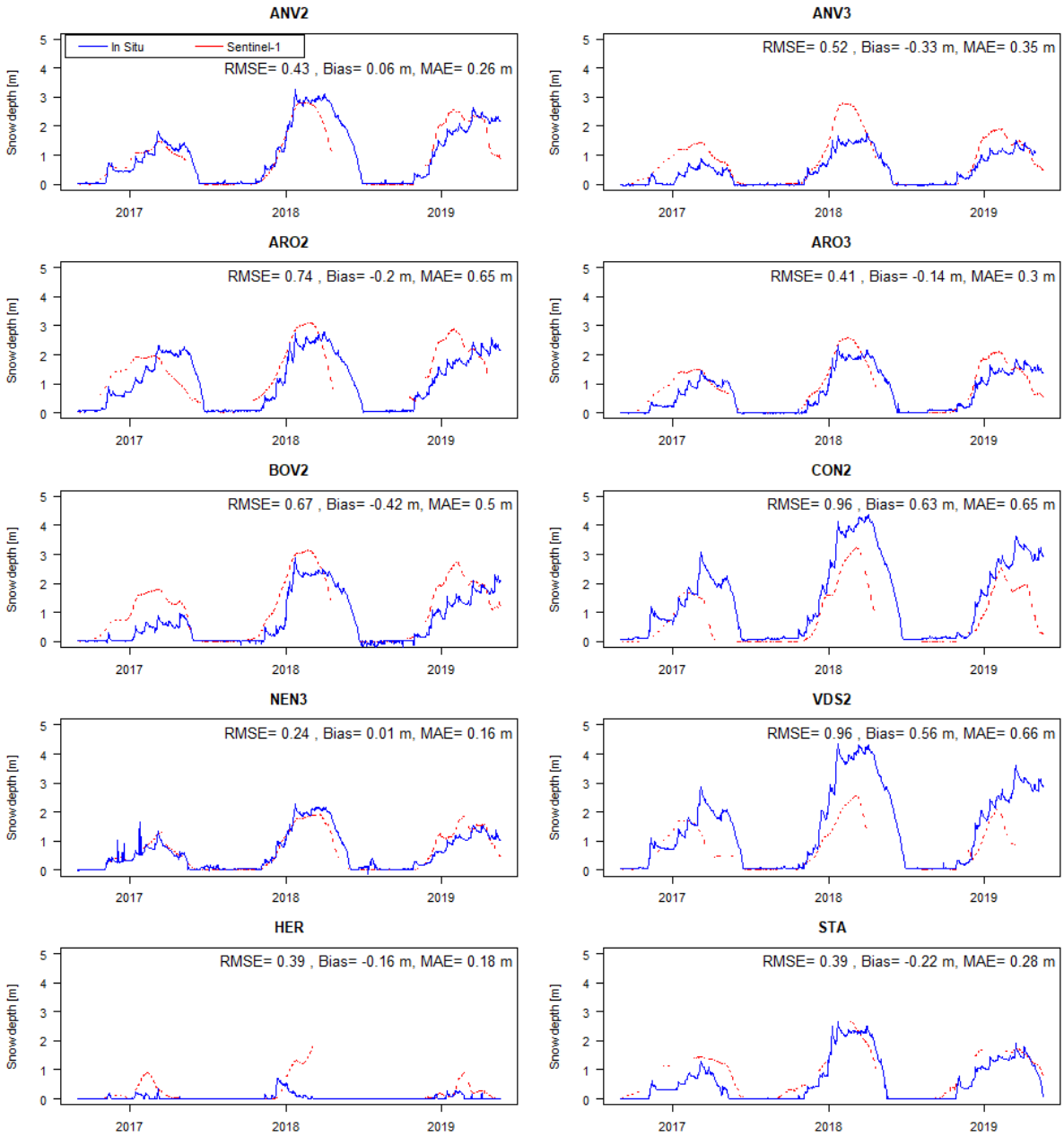

Figure 3: Comparison of the in situ measurements with Sentinel-1 snow depth "base". In situ data from SLF (© 2020, SLF) except for HER (from SMN © 2020 MeteoSchweiz) and STA (from Grande Dixence SA and HYDRO Exploitation SA).

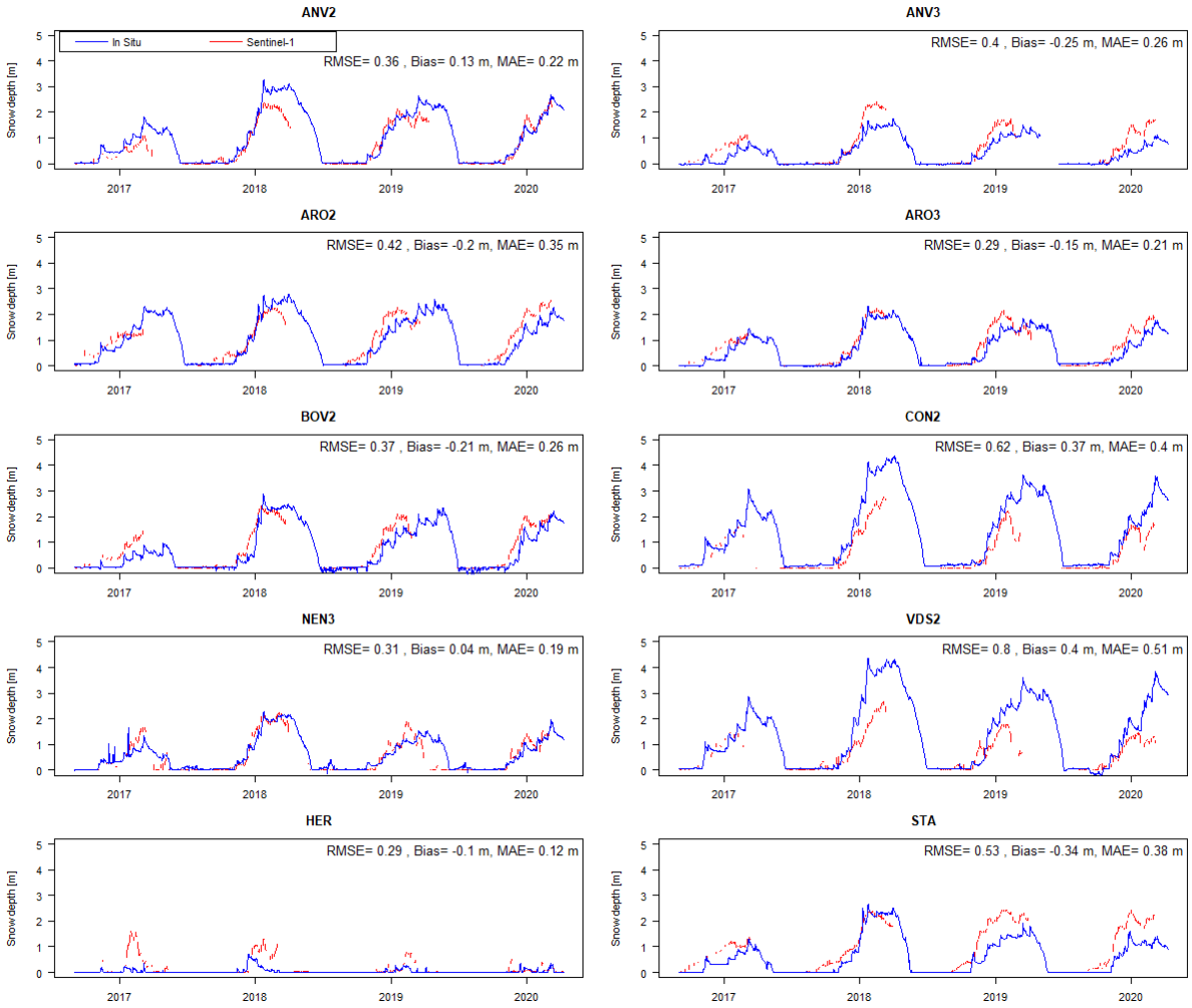

Figure 4: Comparison of the in situ measurements with Sentinel-1 snow depth "exp". In situ data from SLF (© 2020, SLF) except for HER (from SMN © 2020 MeteoSchweiz) and STA (from Grande Dixence SA and HYDRO Exploitation SA).

2.4. Discussion

The two products "base" and "exp" show an acceptable reproduction the dynamics of snow accumulation (Figures 3 and 4). It must be stated that the reliability of the measurements decreases strongly in spring. According to Lievens et al. (2019), this is due to the increased back radiation caused by water particles in the snow cover, which systematically underestimates the snow thickness. Lievens detected these conditions and removed the affected values in the "exp" product. This reduced the error leading to a lower MAE or RMSE for the "exp" product. A visual comparison could not identify the best product, but based on the indicators, the "exp" product was chosen and is used in the next steps of this project.

The average MAE of 0.18 m found by Lievens et al. (2019) is not reached by the average of all ten stations considered in this project. However, the datasets cannot be directly compared, because the time periods of the measurements differ. They only considered the two winters, 2016/17 and 2017/18, while the winters 2018/2019 and 2019/2020 were added in this project. Furthermore, Lievens et al. (2019) used stations from the entire Northern Hemisphere, where much thinner snow depths can be expected compared to alpine snowpacks, and then the MAE is probably smaller at these stations.

Instead of deleting wet snow conditions in spring, the development of new algorithms to correct the snow depth data remains the objective. This would be an important milestone in regard to the use of such satellite data for hydrological models. Until then, using data from mid-March on is in the Alps probably not yet an option.

It remains to be said that the comparison between point measurements and 1 km^2 raster cells is a degree of uncertainty. Furthermore, the range of elevation between the validation stations is limited to 1218 and 2847 masl. However, the Borgne catchment modelled in this project covers a range from 495 to 4357 masl. At high elevation and over glaciers, where in-situ measurements are scarce, almost no in situ snow timeseries exist in Switzerland [Reist & Weingartner (2005)]. In these areas, the reliability of the Sentinel-1 data can only be hardly evaluated.

3. Performance of the original model

3.1. Introduction

This chapter introduces the RS MINERVE software. In the methodology, the two rainfall-runoff models HBV and GSM are explained. It contains also an overview of the input data and the calibration- and calculation setups. The calibrated model is then compared to the operational model from Crealp and main differences and possible problems of the models are discussed. This forms a basis for further improvements proposed in the next chapter.

3.2. Methodology

3.2.1. RS MINERVE

In this project, the modeling software RS MINERVE (RSM) Version 2.8.13.0 [Foehn et al. (2019), García Hernández et al. (2020)] was used. It allows the modelisation of hydrological processes such as snowmelt, glacier melt, surface and underground flow with various options for rainfall-runoff models. The HBV model (by Bergström (1976), Bergström (1992)) was used for non-glacial catchments and the GSM model (by Schaefli et al. (2005)) was used for glacial catchments. They are shortly introduced hereafter. The model for the upper Rhone basin was created and continuously improved within the MINERVE project [Jordan (2007), García Hernández (2011), García Hernández et al. (2014)]. The studied catchment has been divided into subcatchments and elevation bands with a range of a maximum of 500 m.

HBV model

For all non-glacial catchments, the integrated rainfall-runoff model HBV (**H**ydrologiska **B**yråns **V**attenbalansavdelning) was used [Bergström (1976), Bergström (1992)]. The structure of the model is presented in Figure 5a. It contains a snow function, a humidity reservoir and two (upper and lower) soil storage reservoirs. For snowmelt, the classic degree-day factor (DDF) model (Eq. 2) is used [García Hernández et al. (2020)] and computed as follows:

$$M_{sn} = CFMax * (T - TTSM) \tag{2}$$

with M_{sn}: snowmelt $[mm\, d^{-1}]$; $CFMax$: degree-day melting factor $[mm\, °C^{-1} d^{-1}]$; $TTSM$: critical snowmelt temperature [°C]. Snowmelt only occurs when T > TTSM.

GSM model

This semi-distributed model, originally developed by Schaefli et al. (2005), offers the possibility to model the glacier as well as the snow cover (Fig. 5b). GSM stands for **G**lacier and **S**now**M**elt. For both, the snowmelt calculation is performed using a time-varying degree-day snowmelt coefficient (Eq. 3 and 4) [Magnusson et al. (2014), Slater & Clark (2006)]. While snowmelt is limited by the amount of accumulated snow, glacier melt has no volume limit.

$$S' = \max\left(S_{min}; S + \frac{S_{Int}}{2}\sin\left(2\pi\frac{n - S_{Ph}}{365}\right)\right) \tag{3}$$

$$M_{sn} = S' * (1 + b_p * P_w) * (T - T_{cf}) \tag{4}$$

with S': time-varying degree-day snowmelt coefficient $[mm\,^{\circ}C^{-1}d^{-1}]$; S: reference degree-day snowmelt coefficient $[mm\,^{\circ}C^{-1}d^{-1}]$; S_{Int}: degree-day snowmelt coefficient interval $[mm\,^{\circ}C^{-1}d^{-1}]$; n: day of the year [-]; S_{Min}: minimal degree-day snowmelt coefficient $[mm\,^{\circ}C^{-1}d^{-1}]$; S_{Ph}: phase shift of the sinusoidal function [-]; M_{sn}: snowmelt $[mm\ d^{-1}]$; b_p: melt coefficient due to liquid precipitation $[s\,mm^{-1}]$; Pw: liquid precipitation $[mm\,s^{-1}]$; T_{cf}: critical snowmelt temperature $[C]$. Melt only occurs when T > T_{cf}.

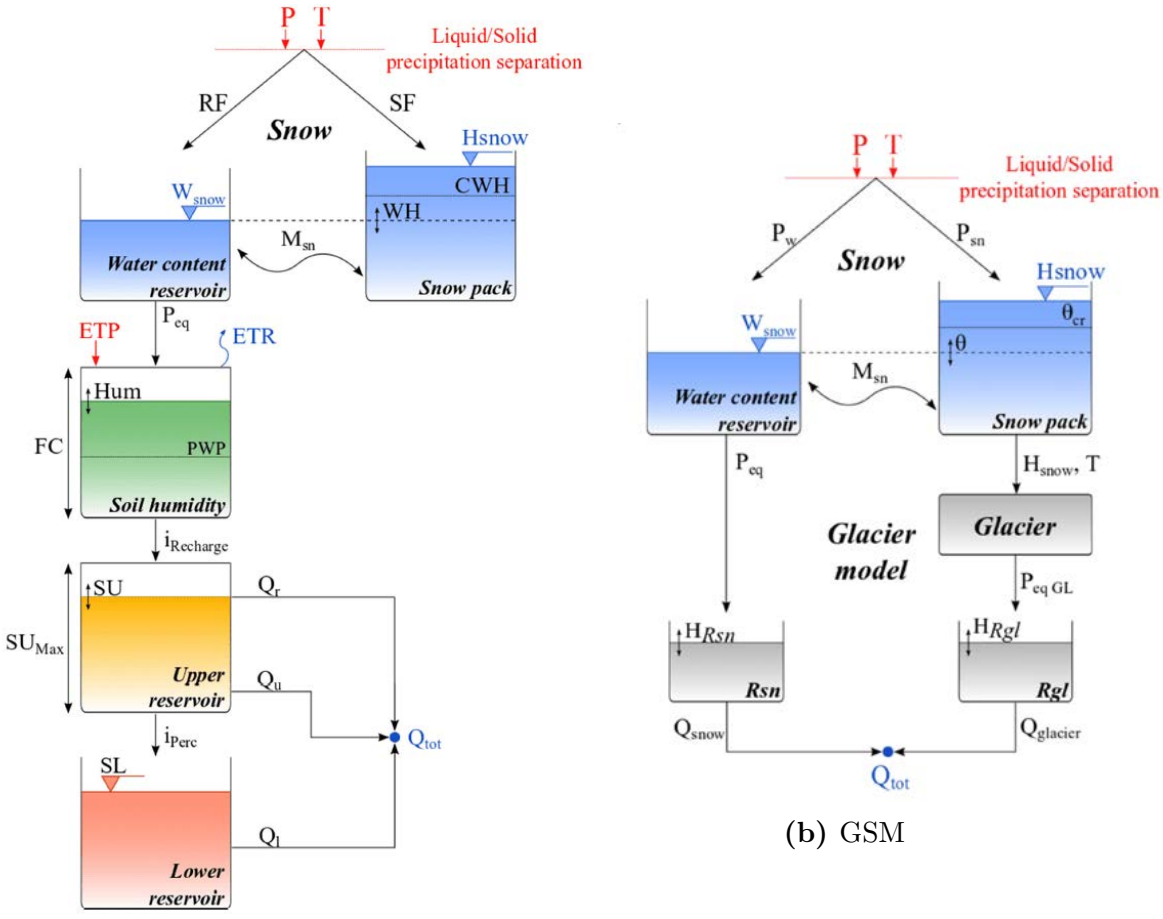

(a) HBV

(b) GSM

Figure 5: The HBV and GSM models (Source: García Hernández et al. (2020)).

3.2.2. Input data

For each subcatchment RSM generates a virtual weather station. For each meteorological input, it interpolates data series of surrounding measuring stations using the Shepard method [Shepard (1968)]. In this study, the weather stations of the SwissMetNet operated by MeteoSwiss were used. Other studies show the advantages and disadvantages of the use of additional data sources such as MeteoGroup Switzerland AG (MG) [Foehn (2019)] or a spatial interpolated product developed by Foehn et al. (2018). Both sources have limited advantages. The MG network has higher measurement uncertainties compared to SMN network and the CombiPrecip product suffers from blind zones due to radar shielding.

SwissMetNet (MeteoSuisse)

Table 3 lists the meteorological stations from the SMN that were used in this study. The station of *Moiry* shows a gap between the first and the 13th of October 2015. For that period of time, the values of the nearest station (*Mottec*) were used. This applies in particular to the rain event on the 6th of October 2015 with a peak of 1.3 mm/10min. For the precipitation station of *Arolla*, four exceptionally high single values were deleted, since there was no visible response observed in flow measurements nearby. Temperature data were visually checked and extreme values were corrected. The temperature station of *Les Attelas* was not considered due to inconsistencies in the series.

Table 3: Meteorological stations of SwissMetNet by MeteoSwiss.

Name	Measured Parameters	X coordinate	Y coordinate	Elevation [masl]
Arolla	P, T	603504	95835	2000
Barrage Grande Dixence	P, T	597255	103580	2164
Bricola	P, T	609887	99430	2440
Evolène	P, T	605415	106740	1825
Fionnay	P	589960	97765	1502
Les Collons	P, T	596041	114169	1772
Moiry	P, T	610169	109590	2127
Mottec	P, T	614325	110730	1580
Nendaz	P, T	590166	107852	1940
Sion	P, T	591630	118580	481
Stafel	P, T	618616	94810	2183
Zermatt	P, T	624350	97566	1638

Discharge stations

The selected area is partly located in the in the extended catchment of the Grande Dixence reservoir. 17 intakes at high elevation are distributed over the area, where the discharge is measured continuously. These measures are operated and provided by Grande Dixence SA and HYDRO Exploitation SA. In addition, two measuring stations of the Canton of Valais, which measure the Borgne in Evolène and Bramois were considered. The Bramois monitoring station is located at the outlet of the catchment perimeter. Based on these measuring stations, the catchment area was subdivided in 10 calibration zones: nine smaller zones, each with one or more associated Grande Dixence measurements, and one larger zone calibrated with the Bramois measurement. The zones as well as the distribution of the Grande Dixence stations is shown in Figure 6. A list of the monitoring sites with the most important parameters is available in Table 4. All data were available for the years 2016 - 2019.

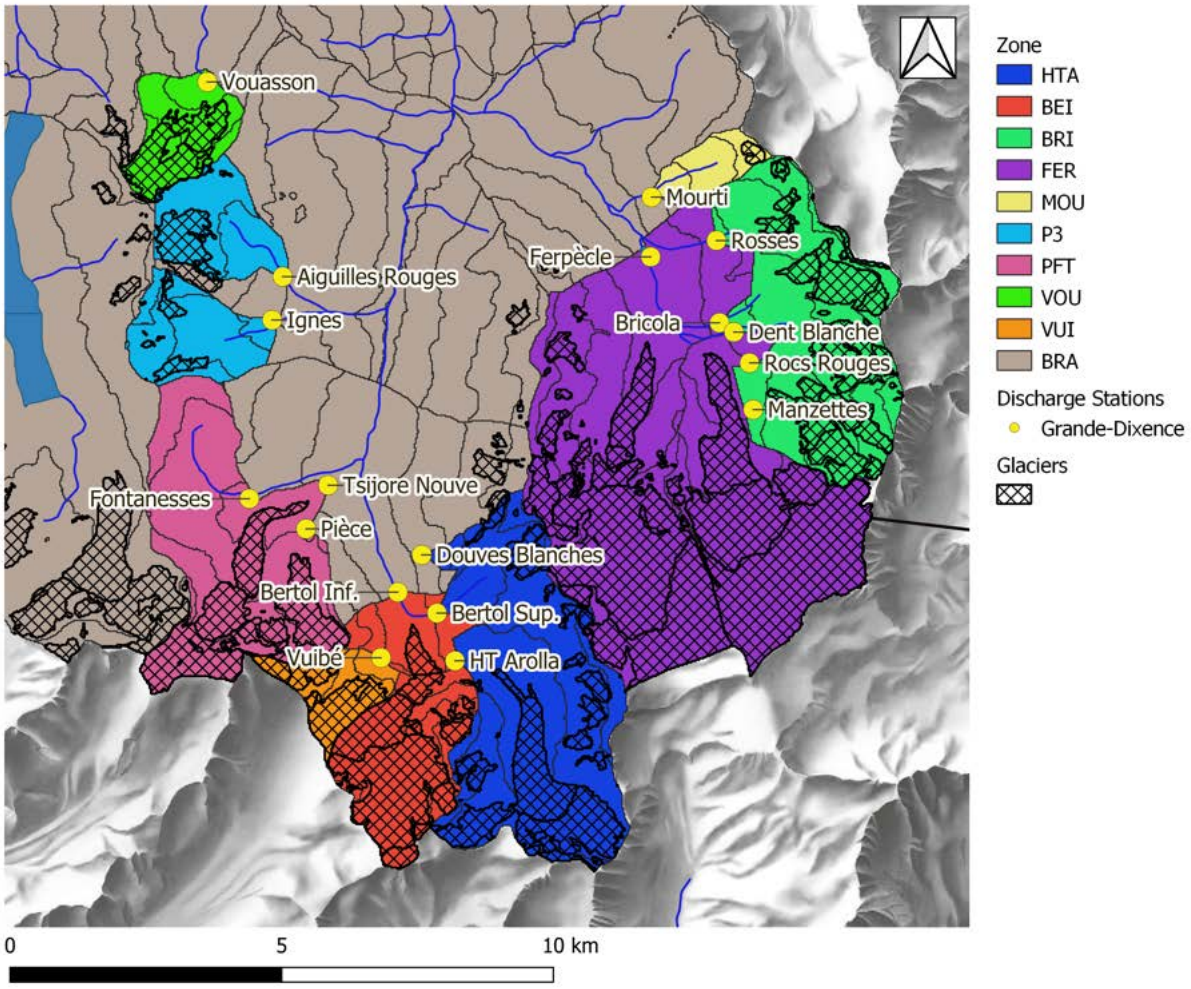

Figure 6: Calibration zones and locations of the discharge measuring stations of the Grande Dixence network (background map: ©2004-2019 swisstopo).

A new ordinance regulates the minimum residual flow rate at the intakes of the BEI and FER zones, starting on the first of January 2019. A flow rate of 200 ls^{-1} must now remain in the river in BEI. In FER, the residual flow rate depends on the season: in the winter period (December to March) 60 ls^{-1} must be provided, in the intermediate period (April and November) 90 ls^{-1}, and in the summer period 200 ls^{-1} (May to October).[1]
All discharge data were visually controlled and zero values were corrected when needed. Because of uncertain data quality, the data of *Mourti* was used only for a short time period between 2017 and 2018. Apart from this, the intake of *Mourti* has a maximal capacity of 0,15 m^3s^{-1} [GrandeDixenceSA (2015)]. The original intention to include the *Evolène* measuring station as a further reference was discarded due to rather poor data quality. The measurement in Bramois is also subject to non-negligible uncertainty. The underlying rating curve was only validated with one measurement until 2020. In particular, it is suspected that winter discharges are overestimated.[2]
The measured turbine flow from Bieudron was available for the entire period. The data from the turbine above Bramois, which has a major influence on the measured discharge regime, have only been measured since the first of July 2017. Data from the two pumping stations *Arolla* and *Ferpècle* were not available for this study.

Table 4: Discharge measuring stations and associated calibration zones.

Name	Operator	Qmean $[m^3s^{-1}]$	Zone
Bertol Inf.	HYDRO SA	0.37	BEI
Bertol Sup.	HYDRO SA	0.12	HTA
Bramois	Canton Valais	7.89	BRA
Bricola	HYDRO SA	0.17	BRI
Dent Blanche	HYDRO SA	0.05	BRI
Douves Blanches	HYDRO SA	0.05	HTA
Evolène	Canton Valais	2.99	-
Ferpècle	HYDRO SA	2.27	FER
Fontanesses	HYDRO SA	0.08	PFT
HT Arolla	HYDRO SA	0.86	HTA
Manzettes	HYDRO SA	0.16	BRI
Mourti	HYDRO SA	0.03	MOU
P3	HYDRO SA	0.32	P3
Pièce	HYDRO SA	0.24	PFT
Rocs Rouges	HYDRO SA	0.07	BRI
Rosses	HYDRO SA	0.09	BRI
Tsijore-Nouve	HYDRO SA	0.29	PFT
Vouasson	HYDRO SA	0.18	VOU
Vuibé	HYDRO SA	0.13	VUI

[1]These numbers are based on the ordinance *"Assainissement des bassins versants de la Matter-Vispa, de la Borgne de Ferpècle et de la Borgne d'Arolla"* of the Canton of Valais, signed on the 3rd of Oct. 2018.

[2]Statements based on intern discussions with T. Brauchli and B. Roquier from Crealp, winter 2021.

3.2.3. Calculation setups

To take the total amount of snow accumulation over one winter into account, the simulation period starts on the first of October 2015. The years 2016, 2017 and 2018 were set as calibration period. The year 2019 served as validation. The simulation time step was set to 10 min and the recording time step to 60 min. Regarding the virtual weather, stations a search radius of 15 km and a minimal number of three stations were chosen. The initial conditions were computed with a one year warm-up. The initial parameters SWEIni [m], HglacierIni [m] and ThetaIni [-] were set to zero at the start of the simulation.

3.2.4. Calibration setups and performance indicators

RS MINERVE has a built-in expert tool to automate calibrations. It allows the simultaneous calibration of different parameters using one or multiple performance indicators. The basis for the calibration were the discharge measurements of the Grande Dixence network in the upper region and the measurement of Bramois at the outflow of the catchment. The different calibration zones (shown in Fig 6) were calibrated separately.

The calibration was carried out between the first of October 2015 and the first of October 2018. The subsequent year 2019 served as validation period. Four parameters of the GSM model and nine of the HBV model, shown in Table 5, were calibrated. The parameters were divided into two groups, which were calibrated one after the other. The first round focused on parameters related to snowmelt. In the second round, the soil parameters of the HBV model were calibrated.

Table 5: Calibrated Parameters of the GSM and the HBV models.

Model	Name [Unit]	Description	Range	Initial value
First Round				
GSM	S [mm°C^{-1}d^{-1}]	Ref. degree-day snowmelt coeff.	0.5-20	5
	G [mm°C^{-1}d^{-1}]	Ref. degree-day glacier melt coeff.	0.5-20	5
	Kgl [d^{-1}]	Release coeff. of glacier melt reservoir	0.1-5	4.5
	Ksn [d^{-1}]	Release coeff. of snowmelt reservoir	0.1-5	4.5
HBV	CFMax [mm°C^{-1}d^{-1}]	Melting factor	0.5-20	5
Second Round				
HBV	Beta [-]	Model parameter (shape coeff.)	1-5	2.5
	FC [m]	Maximum soil storage capacity	0.05-0.65	0.25
	PWP [-]	Soil permanent wilting point threshold	0.03-1	0.5
	SUMax [m]	Upper reservoir water level threshold	0-0.10	0.05
	Kr [d^{-1}]	Near surface flow storage coeff.	0.05-0.5	0.3
	Ku [d^{-1}]	Interflow storage coeff.	0.01-0.4	0.1
	Kl [d^{-1}]	Baseflow storage coeff.	0-0.15	0.02
	Kperc [d^{-1}]	Percolation storage coeff.	0-0.8	0.15

The *Shuffled Complex Evolution – University of Arizona* (SC-ACE) algorithm was used for calibration [Duan et al. (1992), Duan et al. (1993)]. It is based on a synthesis of the best features from several existing algorithms and was designed for solving problems encountered in conceptual watershed models. The well-known Nash-Sutcliffe efficiency (NSE) [Nash & Sutcliffe (1970)] shown in Eq. 5 is chosen as indicator. The NSE is also used for calibrating the operational model by Crealp. It varies between -∞ and 1 and its optimal value is 1[-]. A Nash value below zero indicates that the model has a worse predictive skill than the mean of the measured values. For the validation, three additional parameters were considered:

- The Nash-ln, presented in Eq. 6, represents the NSE for natural logarithmic flow values. It was used to assess differences between low discharge values. The range of the Nash-ln lies between -∞ to 1, with an optimal value equal to 1.
- The relative volume bias (RVB) is showing whether the amount of simulated water corresponds to the measured one (Eq. 7). The optimal value for RVB is zero [-]. A negative RVB indicates that the simulated flows are on average smaller than the measured flows (deficit model) and positive RVB values indicate an overestimation by the model.
- Finally, the Kling-Gupta efficiency (KGE) developed by Gupta et al. (2009) and revised by Kling et al. (2012) has recently become a very popular indicator for hydrological simulations. It takes correlation, bias and variability into account (Eq. 8a - 8c). Similar to the NSE, it varies between -∞ and 1 and its optimal value equals 1. For KGE above -0.41, the model has a better predictive skill than the average of the measured values [Knoben et al. (2019)].

$$Nash = 1 - \frac{\sum_{t=t_1}^{t_f}(X_{sim,t} - X_{ref,t})^2}{\sum_{t=t_1}^{t_f}(X_{ref,t} - \overline{X}_{ref})^2} \tag{5}$$

$$Nash - ln = 1 - \frac{\sum_{t=t_1}^{t_f}(ln(X_{sim,t}) - ln(X_{ref,t}))^2}{\sum_{t=t_1}^{t_f}(ln(X_{ref,t}) - ln(\overline{X}_{ref}))^2} \tag{6}$$

$$RVB = \frac{\sum_{t=t_1}^{t_f}(X_{sim,t} - X_{ref,t})}{\sum_{t=t_1}^{t_f}(X_{ref,t})} \tag{7}$$

$$KGE = 1 - \sqrt{(r-1)^2 + (\beta-1)^2 + (\gamma-1)^2} \tag{8a}$$

$$\beta = \frac{\mu_{sim}}{\mu_{ref}} \tag{8b}$$

$$\gamma = \frac{CV_{sim}}{CV_{ref}} = \frac{\sigma_{sim}/\mu_{sim}}{\sigma_{ref}/\mu_{ref}} \tag{8c}$$

with X_{sim}: modelled values; X_{ref}: measured values; r: correlation coefficient between simulated and reference values [-]; β: bias ratio [-]; γ: variability ratio [-]; μ: mean discharge $[m^3 s^{-1}]$; CV: coefficient of variation [-]; σ: standard deviation of discharge $[m^3 s^{-1}]$.

The indicators were calculated for a period from the first of October 2015 until the 30th of September 2018 for the calibration period and from the 1st of January 2019 until the 31th of December 2019 for the validation period. For the calculation of all indicators in RStudios, the *hydroGOF* package[1] was used.

3.2.5. Sensitivity analysis

To show the influence of the different calibrated parameters, a short sensitivity analysis was performed for the calibration zone BRI. For this purpose, the model behavior was investigated when individual parameters were reset to the initial value. The resulting discharge was then plotted together with the fully calibrated and the measured discharge. A control period starting on the 30th of May 2019 and going until the 9th of July 2019, representing the snowmelt period, was chosen. The differences were assessed visually.

3.3. Results

Table 6 contains the NSE coefficients for the station of Bramois and the average value of the 10 discharge stations located upstream. The newly calibrated model clearly outperforms the operational one, for both the calibration and the validation period.

Hereafter, the results of the two models are analysed in more detail. First the hydrographs in Bramois are presented. Then, the modelled SWE values are compared to the SWE estimates derived from Sentinel-1 snow depths applying the conversion by Jonas et al. (2009). Finally, the results from the sensitivity analysis of the BRI zone are shown.

It is surprising that the BEI zone showed an inferior Nash value (0.22) during the validation period. The RVB varies strongly between the calibration period (0.02) and the validation period (0.67). This is most likely due to the new regulation of residual waters from the 1st of January 2019. This limitation induces larger errors in the model. To improve this, an adjustment of the relation between the incoming discharge an the residual flow should be made for further application. This was not feasible within the framework of this project. As a consequence, the performance indicators of the BEI zone were excluded for the validation period for further investigations in this project.

Table 6: Nash-Sutcliffe efficiencies (NSE) of the operational and the calibrated models in Bramois and average of NSE of the 10 upstream discharge stations for the calibration and the validation periods.

	Configuration	Calibration	Validation
Bramois	Operational	0.56	0.76
	Calibrated	0.79	0.80
Mean of the zones	Operational	0.69	0.59
	Calibrated	0.83	0.76

[1] 'hydroGOF' version 0.4-0

Station of Bramois

Measured and modelled discharge in Bramois are shown in Figure 7 for the operational and the calibrated model. Three elements are highlighted in this figure: Firstly, the flow rates are generally better reproduced by the calibrated model, especially during the snowmelt periods (visible in spring 2016 and 2018). Secondly, the calibrated model seems to underestimates the winter runoff. It should be mentioned that the discharge observations in Bramois overestimate the winter base flow[1]. Thirdly, the calibrated model has problems reproducing some summer peaks. At the same time, some of those peaks are largely overestimated by the operational model. The calibration leads to a slightly larger underestimation of the total water volume. It appears that the RVB decreased from -0.04 to -0.09 for the calibration period and from -0.07 to -0.12 for the validation period.

Comparison MINERVE and Sentinel-1

To pinpoint possible problems of the calibrated model, the modeled SWE are compared to SWE values derived from Sentinel-1 "exp" data on the 4th of March 2018 (Figure 8). This last product is the best estimate of spatially distributed SWE available. However, one has to keep in mind that these estimates are subject to non negligible uncertainties. Another comparison is given in Appendix A.1 for the 4th of March 2017. There are large differences between the modelled and observed SWE values. In general, the differences increase at higher altitude, with clear underestimation in the hydrological model. The scatterplot does not indicate a clear linear relation, neither for the HBV- nor for the GSM models. It is remarkable that in the MINERVE model only few points exceed a SWE value of 0.5 m. The modelling of deeper a snowpack seems somehow limited.

Sensitivity analysis

The sensitivity analysis shows that most parameters have limited influence on the flow regime. Exceptions are the *release coefficient of glacier melt reservoir (Kgl, GSM)* and the *baseflow storage coefficient (Kl, HBV)*, shown in Figure 9. The hydrographs of the other parameters and a table with the initial and calibrated parameters are shown in Appendix A.2.

Kgl (GSM) has a direct linear influence on the melt water released from the glacier. The significantly lower daily peaks in the calibrated model show that *Kgl* causes the daily hydrograph to flatten considerably from the 24th of June 2019 on. The reason, why the calibration tends to a *Kgl* value which causes a flattening of the daily hydrograph, is unclear. Foehn et al. (2020) has noted similar tendencies, albeit for much larger catchments. He suspected an attempt of the model to compensate for inaccuracies in the time lag.

The variation of *Kl (HBV)* causes flow rate changes, especially during the early melting phase. The calibrated Kl value (0.04 d^{-1}) results in a higher hydrograph. The calibrated model thus approaches the measured meltwater discharges more closely compared the initial value. This is due to the fact that a higher *Kl* results showing less infiltration of water into the subsurface. This could lead to an underestimation of water volume later in the year. Whether this underestimation is the reason for the overcompensation of the

[1]Statement based on intern discussion with T. Brauchli from Crealp, winter 2021.

Kgl parameter, can only be speculated. In any case, it could be due to underestimated snow volumes.

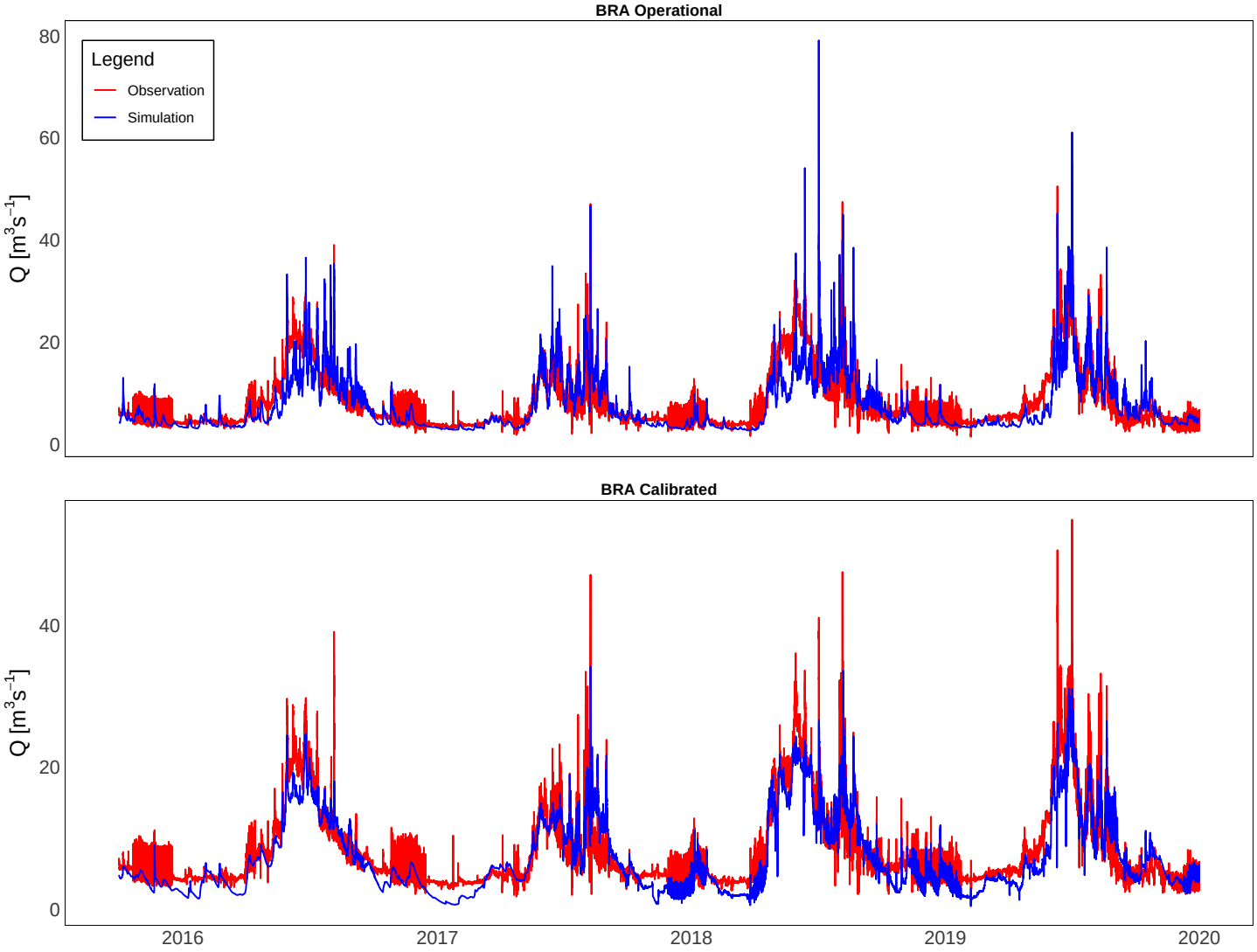

Figure 7: Flow hydrograph of the Bramois station for the operationel (upper) and the calibrated (lower) configuration.

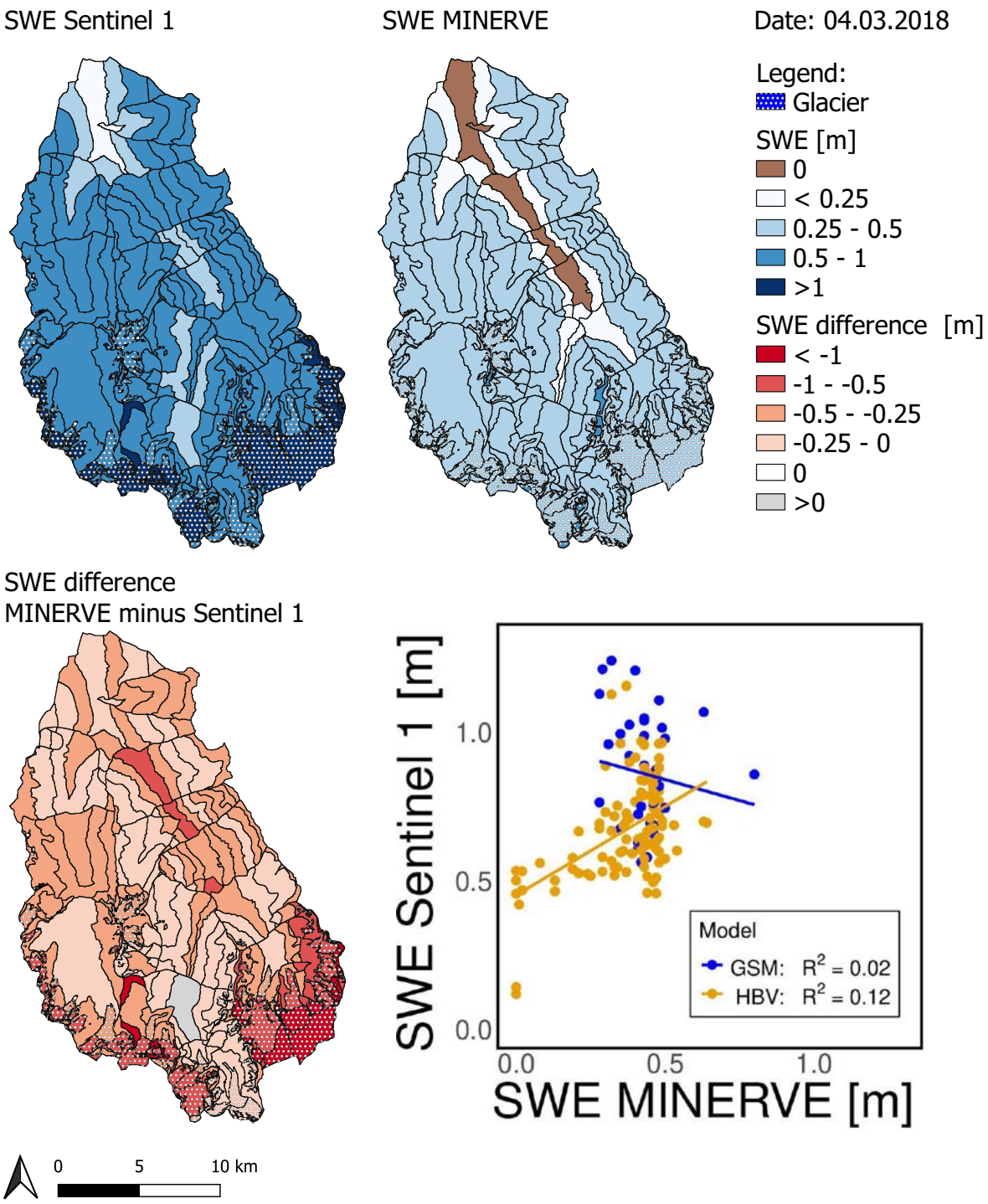

Figure 8: Comparison of modelled snow water equivalent (SWE) with SWE derived from Sentinel 1 snow data for the 4th of March 2018. The upper plots show the absolute SWE values for both Sentinel-1 (top left) and the calibrated MINERVE model (top right). The difference of the two is shown on the bottom left (MINERVE minus Sentinel-1). The scatter plot on the bottom right shows MINERVE and Sentinel-1 derived SWE grouped by the two models (GSM and HBV).

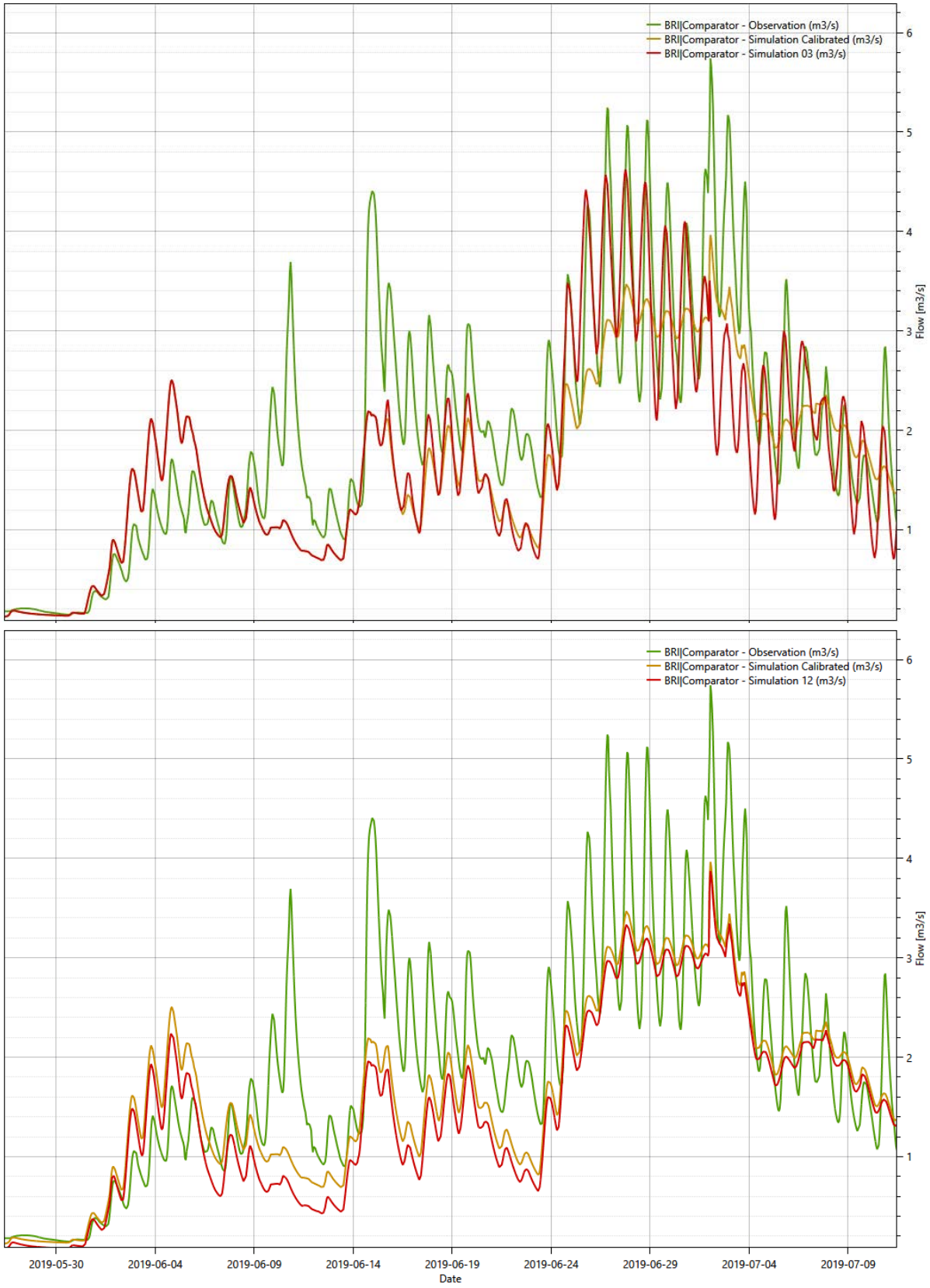

Figure 9: Flow hydrograph of the melting period in 2019 of the BRI catchment, comparing the measured discharge (green), the calibrated discharge (orange) and the calibrated discharge with an adjustment of the parameter Kgl (upper plot) or Kl (lower plot) to its initial value (red).

3.4. Discussion

The new calibration of the model clearly improves the model performance regarding the NSE. This is the case for the station of Bramois and even more for the upper zones. The flow dynamics are throughout better reproduced by the calibrated model. However, the hydrograph in Bramois points out certain downsides of the calibration. On one hand, the summer peaks are not as well reproduced by the calibrated model as they are by the operational one. The calibrated model tends to underestimate the peaks. The reason for this could not be clearly identified. The uncertainty of the measurement in Bramois is a limiting factor for drawing any stricter conclusions. On the other hand, the calibrated model underestimates the winter base flow. This statement must be treated with caution, as the base flow in winter is overestimated in the observation. A manual measure from the 9th of March 2021 gave a value of 2 m^3s^{-1}.[1] The observation used in this project showed an average winter baseflow of arround 4 m^3s^{-1}. The rating curve will be improved in the near future, by performing new salt gauging. This is a prerequisite to any further analysis. The observations from the Dixence network are quality checked by HYDRO Exploitation SA on a regular basis. They expect measurement uncertainties lower than 5%.[2]

An underestimation of peak runoffs occurred in some of the upper zones as well. The sensitivity analysis showed that this is only induced by few parameters. For an operational use of the model, these parameters, primarily *Kgl* (GSM model), should be adjusted manually.

The comparison of SWE modelled with RS MINERVE and the SWE derived from Sentinel-1 data showes large differences. Even though the uncertainties of both datasets are probably substantial, it shows that the MINERVE model is not able to reproduce high SWE values. In Avanzi et al. (2020), they derived SWE values from snow-course data for the valley of Aosta, which borders the perimeter of this project on the south. They found that even in May 2018 SWE values over 1 m occurred above 2000 masl. This supports the hypothesis, that SWE is underestimated by the MINERVE model, especially at high elevation. An underestimation of modelled SWE using interpolated meteorological observations is coherent with what can be found in the literature [Gugerli et al. (2020), Foehn et al. (2020)].

[1] Statement based on intern discussion with T. Brauchli from Crealp, winter 2021.

[2] Statement based on email conversation between M.Hurni and C. Constantin, HYDRO Exploitation SA, autumn 2020.

4. Performance of the improved model

4.1. Introduction

Two approaches to improve the model performance are investigated in this chapter. On one hand, a more sophisticated snow melt model including short wave radiation and surface albedo was integrated. On the other hand, Sentinel-1 snow data were assimilated.

Various studies show that on glaciers net shortwave solar radiation is the dominant source of melt energy [Braithwaite & Olesen (1990), Arnold et al. (1996), Greuell & Smeets (2001), Willis et al. (2002)]. At the same time, the melting of snow and ice is often modeled using a simplified degree day factor (DDF) approach [for example Foehn et al. (2020)]. Pellicciotti et al. (2005) compared different melt models applied on the glacier of *Arolla*, by chance within the project perimeter. They showed that the most promising results are obtained with the *additive* model in *Arolla*. This model extends the DDF formulation with an additional term that takes short wave radiation into account. Using radiation measurements from MeteoSwiss stations, this model could also be applied in this project. Averaging the values of different measuring stations is not optimal regarding the strong dependence of the solar radiation on slope and aspect of the catchment. However, Comola et al. (2015) showed that above a catchment surface of 7 km^2, the impact of the aspect is not significant. Three of the ten calibration zones defined in this project fall below this threshold; MOU [1.6 km^2], VOU [3.4 km^2] and VUI [2.3 km^2].

The idea of including remotely sensed snow data into hydrological modeling is not new but highly pertinent (see for example Foehn et al. (2020), Vögeli et al. (2016), Baba et al. (2018) or Avanzi et al. (2020)). Baba and Avanzi explicitly suggest the use of Sentinel-1 derived snow depth data as an interesting area of investigation.

The validation of Lievens's product in Chapter 2 gives reason to hope that the modelling problems identified in Chapter 3 can be improved. Since Lieven's product is open-source and available in near-real-time, a regular assimilation in the operational MINERVE model would be feasible.

In addition to the previously used performance indicators, a validation with MODIS data is carried out. This illustrates the differences between the models and a reliable remotely-sensed product during the melting period.

4.2. Methodology

To guarantee comparability with the calibrated model from the previous chapter, the same settings and parameters were chosen whenever possible. The only additions were the radiation parameters and the assimilated SWE. The assimilated model could no longer be calibrated the same way. All changes are described hereafter.

4.2.1. Radiation

To consider the solar radiation, the equations for the melt rate were modified according to the *additive* model by Pellicciotti et al. (2005).[1] In addition to the conventional DDF term, the new equation (Eq. 9) uses a further term that takes direct solar radiation into account.

$$M = TF * T + SRF(1 - \alpha)Rad \tag{9}$$

with: M: melt rate $[mm\ d^{-1}]$; TF: temperature factor $[mm\ ^{\circ}C^{-1}d^{-1}]$ corresponds to S' for GSM or $CFMAX$ for HBV; T: Temperature $[^{\circ}C]$; SRF: shortwave radiation factor $[m^2mmW^{-1}d^{-1}]$; α: Albedo [-]; Rad: global radiation $[Wm^{-2}]$.

Incoming shortwave radiation series were taken from seven SMN-stations listed in Table 7. Reflected shortwave radiation (= albedo) was calculated using Brock's empirical formula for snow albedo [Brock et al. (2000)]. Ice albedo is assumed to be constant at 35%.

The extension of the model led to an additional parameter SRF $[m^2mmW^{-1}d^{-1}]$ for the HBV model. Regarding the GSM model, there were two additional parameters: SRF $[m^2mmW^{-1}d^{-1}]$ for snow and IRF $[m^2mmW^{-1}d^{-1}]$ for ice. These three parameters were added to the first calibration round. The other calibration settings remained the same as described in Chapter 3.2.4. The designation "RAD" is used for this configuration from now onwards.

Table 7: The measuring stations for incoming shortwave radiation from the SwissMetNet.

Name	X coordinate	Y coordinate	Elevation [masl]
Evolène / Villa	605412	106748	1825
Gornergrat	626900	92512	3129
Les Attelas	586854	105302	2734
Montana	601709	127488	1422
Mottec	614325	110730	1580
Sion	591633	118583	482
Zermatt	624298	97574	1638

4.2.2. Data assimilation

For the data assimilation, the data from Sentinel-1 "exp" is used (described in more detail in Chapter 2.1). Assimilation is carried out on nine selected dates, three each year from 2017 until 2019. For this purpose, the measured snow depths were averaged over the polygons of the altitude bands. To make the conversion from snow depth to SWE, the model by Jonas et al. (2009) is used. These values are then assimilated into the model by adjusting the state variables SWE. To achieve this, RS MINERVE was run remotely from RStudio. Unfortunately, this type of modelling does not allow a continuous calibration

[1] the changes in the software were implemented by T. Brauchli, Crealp 2020.

over several years, as data assimilation can become complicated during the calibration period. Therefore, the calibration was carried out separately for the years 2017 and 2018. The resulting parameter sets were evaluated individually.

Various arguments played a role in the choice of assimilation dates. Ideally, the closest date to the peak of accumulation should have been chosen for each catchment. As shown in Chapter 2, the quality and coverage of the Sentinel-1 data decreases strongly when snowmelt occurs in spring. Data assimilation after the beginning of March was therefore not considered as an option. An assimilation too early in the accumulation period makes little sense, as the deviation to the peak of accumulation is still large. Furthermore, one has to keep in mind that the revisit time of the Sentinel-1 satellite is 6 days. Following dates were chosen for assimilation: 03.02.2017; 13.02.2017; 04.03.2017; 08.02.2018; 20.02.2018; 04.03.2018; 03.02.2019; 17.02.2019; 27.02.2019.

The data assimilation always took place at noon. Two calibration periods were chosen: DA17 = 04.03.2017 - 04.03.2018 and DA18 = 04.03.2018 - 04.03.2019. The same parameters were calibrated for the same areas with the same indicator as in Chapter 3.2.4. The validation period was still the year 2019. The two data assimilations were also performed for the radiation model described in the previous chapter. Together with a radiation-only version, five configurations are thus obtained:

- RAD = Regular model including the new additive radiation equation.
- DA17 = Assimilated model calibrated from 04.03.2017 - 04.03.2018
- DA18 = Assimilated model calibrated from 04.03.2018 - 04.03.2019
- RAD+DA17 = Assimilated model calibrated from 04.03.2017 - 04.03.2018, including the new additive radiation equation.
- RAD+DA18 = Assimilated model calibrated from 04.03.2018 - 04.03.2019, including the new additive radiation equation.

4.2.3. MODIS validation

For an additional validation, the snow covered area product from the Moderate-Resolution Imaging Spectroradiometer (MODIS) was used. The MODIS product is combination of two series of measurement by the satellites Aqua and Terra called MYD10A1 and MOD10A1 (version 6) [Hall et al. (2015a), Hall et al. (2015b)]. It provides a daily value of the Normalized Difference Snow Index (NDSI), related to the presence of snow in a pixel [Hall et al. (2002)]. The NDSI varies from 0 (no snow) to 100 (complete snow cover). The spatial resolution is 500 m. For the comparison, both the NSDI and the modelled SWE were transformed into a binary "snow" or "no snow" variable. NSDI values below 25 were considered as "no snow". This threshold was proposed by Parajka & Blöschl (2008) and used by Foehn et al. (2020) to minimise the error of snow overestimation and underestimation. The variable derived from MODIS was compared with the calculated SWE from the different configurations on multiple dates in spring 2019. In RS MINERVE, all modelled SWE values above 0 m were considered as "snow".

4.3. Results

The configurations introduced in this chapter were compared to the two models in Chapter 3. For the sake of consistency, the designation of the second model remains "calibrated" even though the five added configurations were recalibrated as well. First in this chapter, the performance indicators are compared for the upper zones as well as for the station of Bramois. Then the hydrographs for the Bramois station are presented. Finally, the results from the validation with MODIS snow cover data are shown.

Performance Indicators

Figure 10 shows NSE for calibration and validation periods for all configurations. It has to be mentioned that not all configurations have the same calibration period (see Chapters 3.2.4 and 4.2.2). The addition of solar radiation leads to an improvement of NSE values for almost all of the upper zones compared with the "calibrated" model. This shows the gain of extending the model with solar radiation observations. To some extent, this is also true for the RVB shown in Figure 11. The boxplots for Nash-ln and KGE are shown in Appendix A.3.

Regarding the assimilated models, the situation is less straightforward. For the calibration period, some of the zones show very high NSE values regarding the DA18 and RAD+DA18 models. However, for the validation period they are lower. When looking at the DA17 and RA+DA17 models, there are relatively large spreads in both periods. In general, the assimilated models tend to a higher RVB. The choice of the year (2017 or 2018) had a strong influence on the calibration and the results.

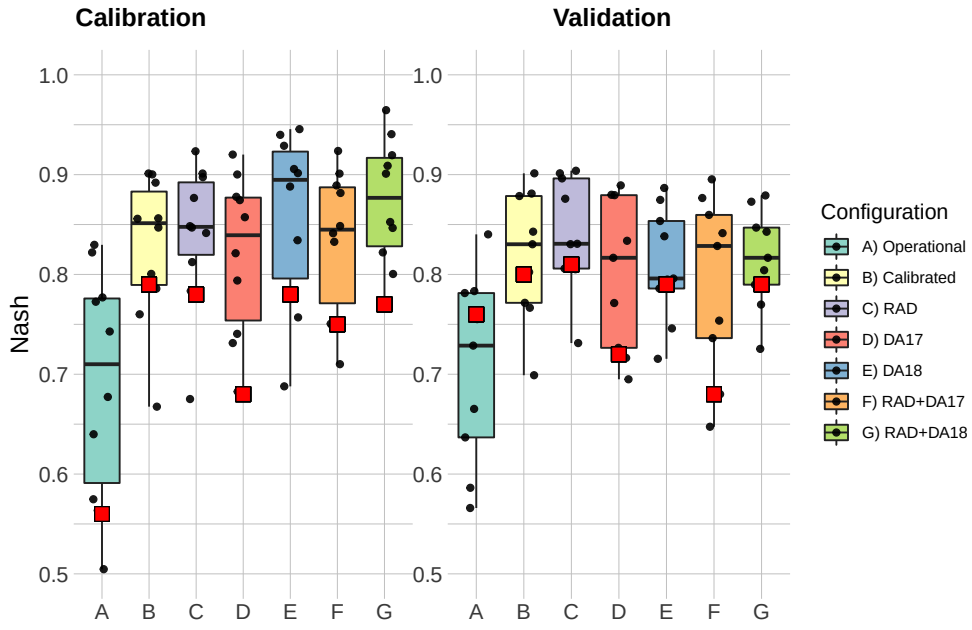

Figure 10: NSE of the seven model configurations (A-G) for the calibration and the validation periods. The boxplots represent the median (bold horizontal line) and the 25 and 75 quantiles (hinges) for the indicators of the ten calibration zones (without BEI for the validation). The red square indicates the value for the station of Bramois.

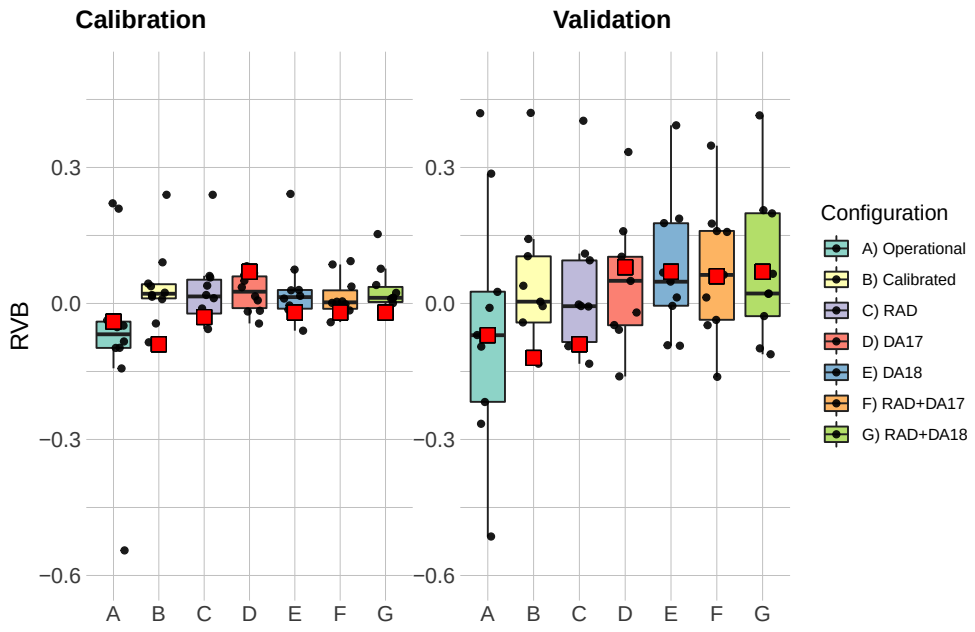

Figure 11: Relative volume biases (RVB) of the seven model configurations (A-G) for the calibration and the validation periods. The boxplots represent the median (bold horizontal line) and the 25 and 75 quantiles (hinges) for the indicators of the ten calibration zones (without BEI for the validation). The the lower and upper whiskers extend from the hinge to the largest value no further than 1.5 * inter-quartile range from the hinge. The red square indicates the value for the station of Bramois.

Station of Bramois

The performance indicators for the station of Bramois are marked as red squares in Figures 10 and 11. None of the models is strictly outperforming the others. RAD shows the best performance for the validation period. NSE values showed great differences between the calibration years 2017 and 2018. Regarding the RVB, a clear difference between the configurations A-C and D-G is visible. While the first three models tend to underestimate the water volume, the latter four tend to an overestimation. This could be due to an overestimation of snow estimates by the Sentinel-1 product. All calibrated parameters for the BRA zone are found in Appendix A.4 and numerical values of all four indicators are found in Appendix A.5.

The hydrograph for the RAD model is shown in Figure 12. It underestimates the summer peaks and the winter baseflow, similar to the "calibrated" model. The hydrographs of the four assimilated models are shown in Figure 13. Neither of them is able to accurately reproduce the summer peaks. DA17 matches the winter base flow best but the flow rate in summer is too small. DA18 matches the summer discharges better. However, here we find an overestimation of the early snowmelt related discharges in spring 2017 and 2019. The two combined models RAD+DA17 and RAD+DA18 resemble their corresponding model without consideration of solar radiation. As discussed in Chapter 3, the uncertainties of the measurement in Bramois is a limiting factor for further conclusions that has to be remedied in the future.

MODIS validation

The simulated snow cover extent was compared with the binary snow variable derived from MODIS data. Figures 14 and 15 show the results for the four configurations "calibrated", RAD, DA17 and DA18 on the 30th of March 2019 and on the 29th of June 2019. In the Appendix A.6, a similar plot on the 4th of June 2019 and the results for the RAD+DA17 and RAD+DA18 configurations can be found. They show an underestimations of the snow covered area by two models "calibrated" and RAD. This is coherent with the findings in Chapter 3 and with the negative RVB in Bramois for these two configurations. The assimilated models tend to an overestimation of the snow covered area. Here as well, there are some differences between the two assimilation configurations: DA17 tends to a larger overestimation.

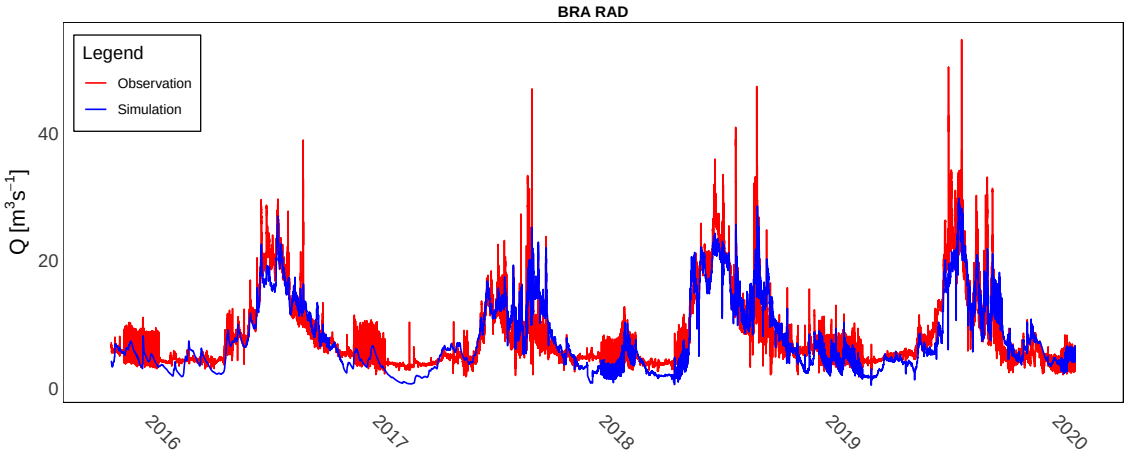

Figure 12: Flow hydrograph of the Bramois station for the RAD configuration.

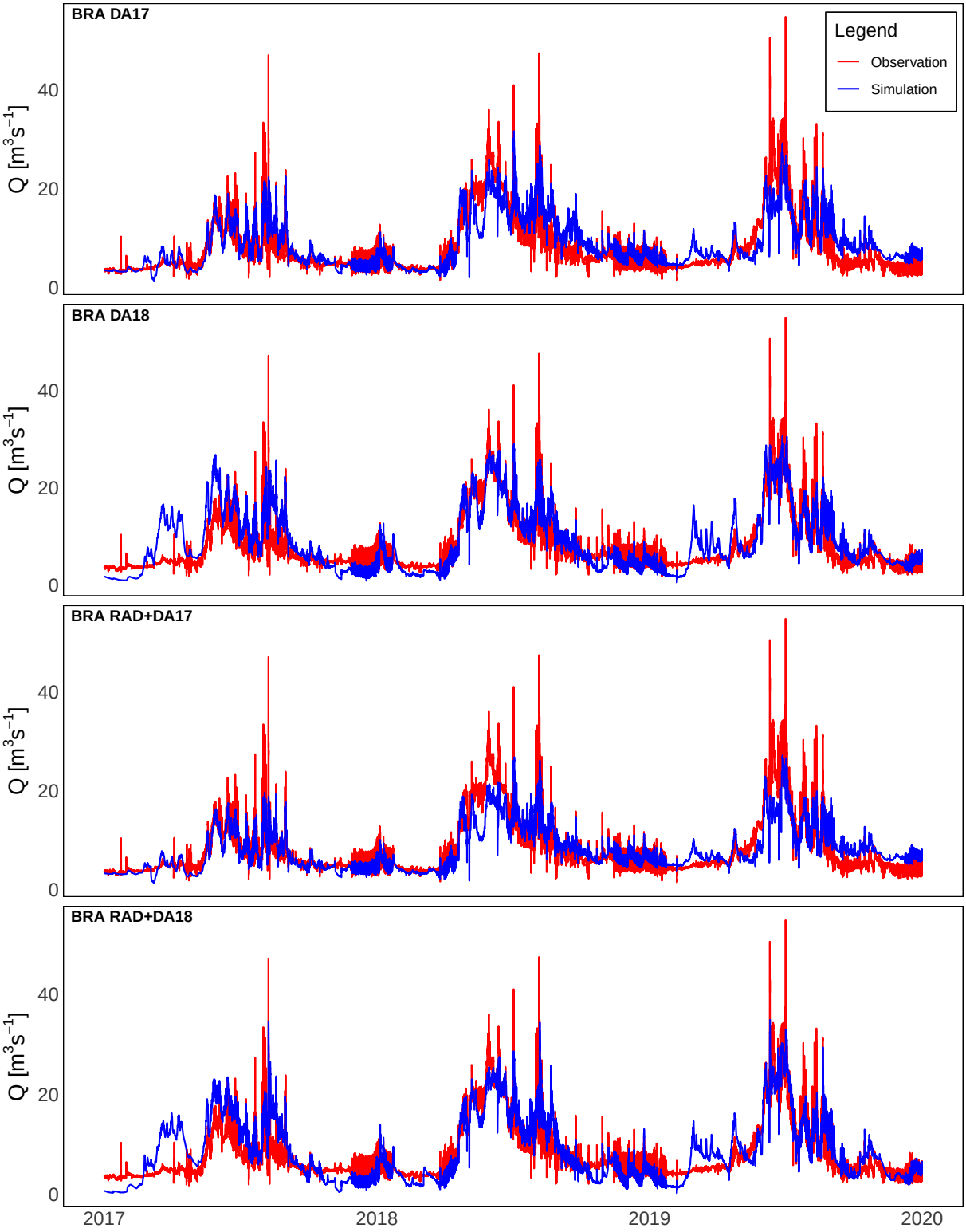

Figure 13: Flow hydrograph of the Bramois station for the four data assimilated configurations.

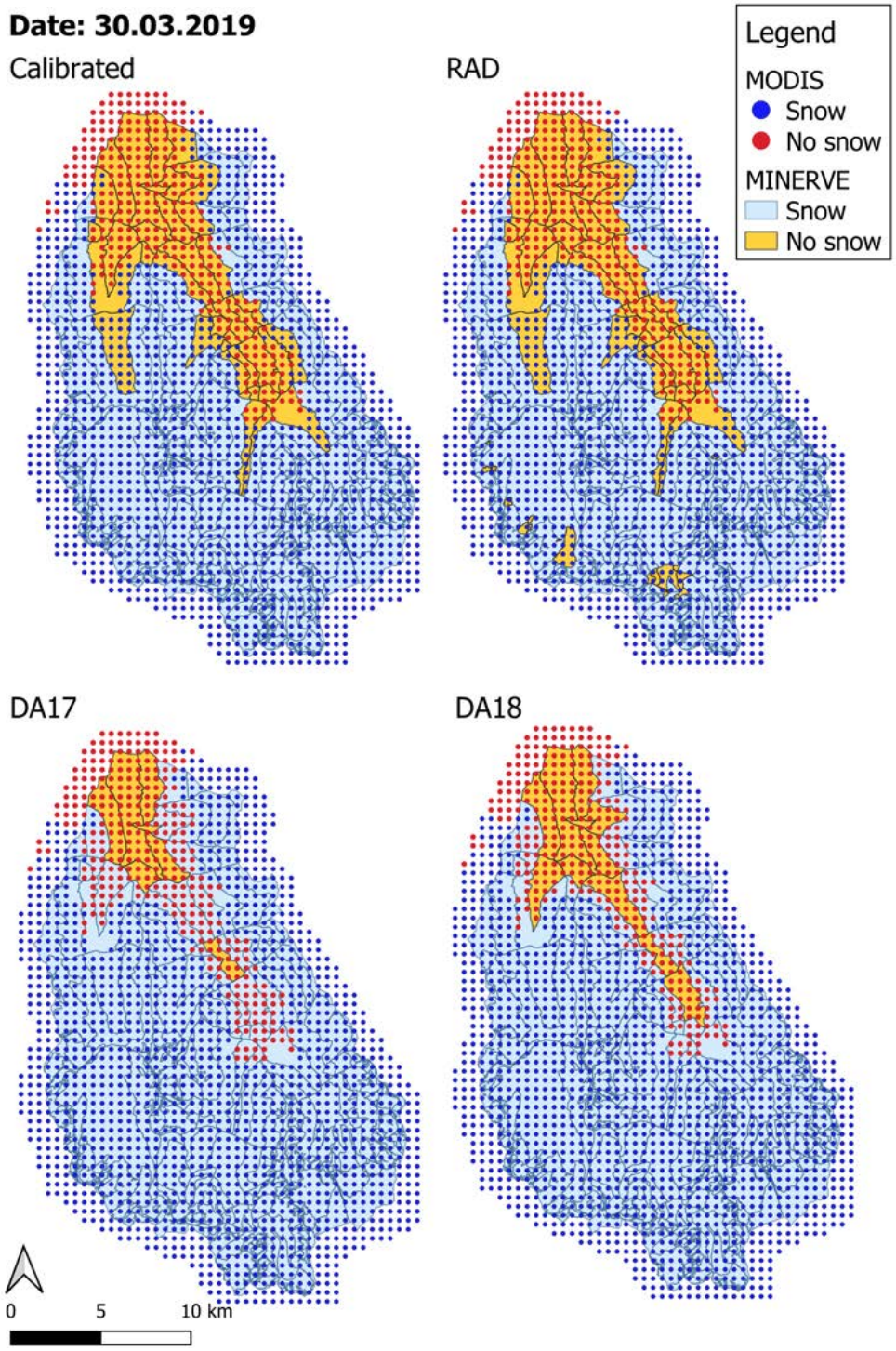

Figure 14: Modeled snow cover of four configurations on the 30th of March 2019 compared to observed snow cover by MODIS.

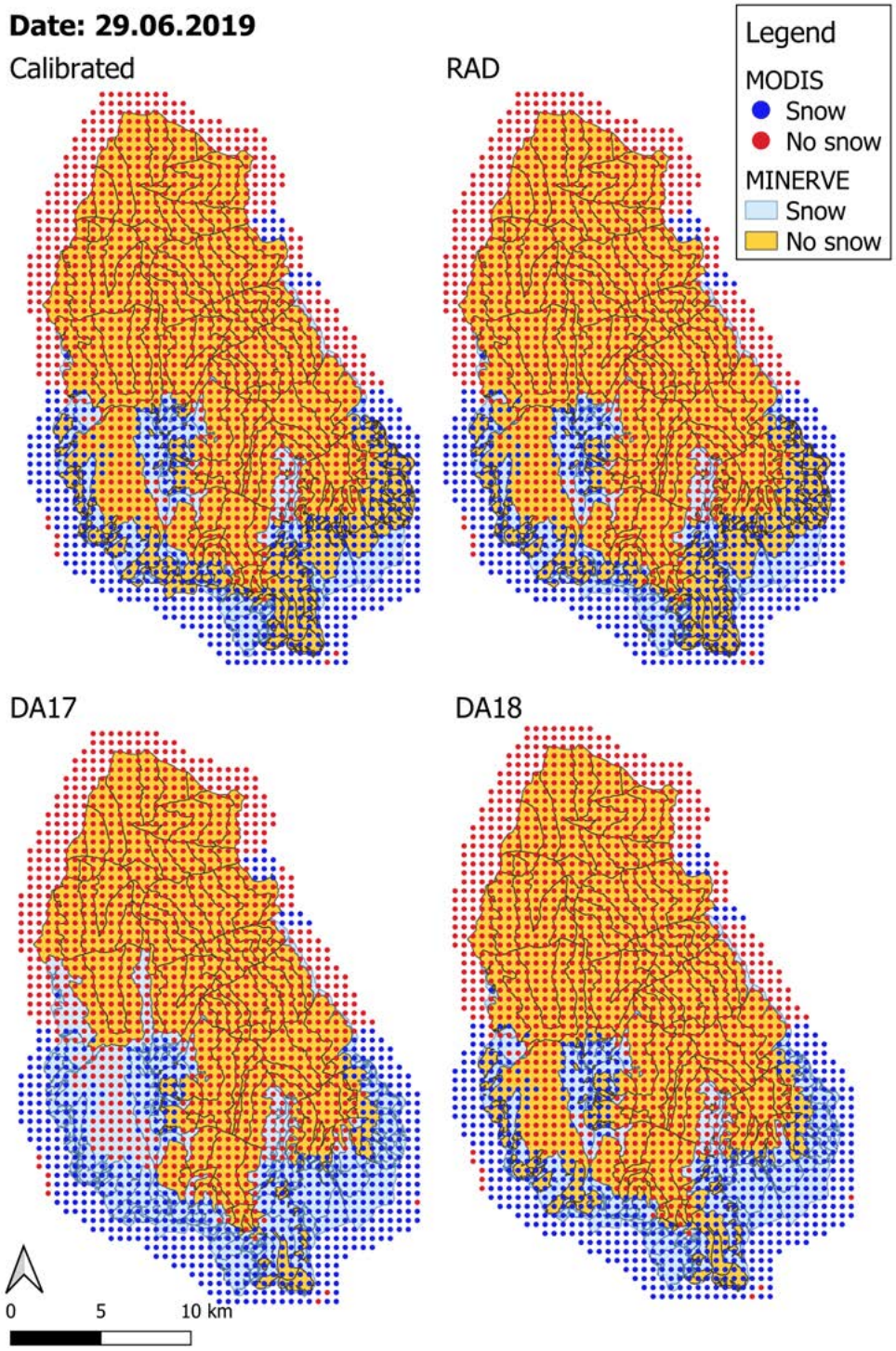

Figure 15: Modeled snow cover of four configurations on the 29th of June 2019 compared to observed snow cover by MODIS.

4.4. Discussion

The integration of the solar radiation improves the model performance in particular for the upper zones. In these areas, snow is present during most of the year. This means that the impact of snowmelt on the hydrograph is more important. Therefore, the addition of solar radiation has a larger effect. An extension of the model is thus particularly recommended for high elevated catchments. The lower NSE value of the RAD model compared with the "calibrated" model for the station of Bramois indicates, that the calibration found a local maximum. At the same time, RAD shows the highest NSE for the validation period at this station. This shows on one hand the positive effect of this new model on the considered indicators. On the other hand, it shows the risk of finding a local maximum when calibrating many parameters at the same time.

The data assimilation leads to an overestimation of modeled water volumes, especially for the Bramois station. Because non-assimilated models tend to underestimate the water volumes, it is presumed that the truth lies between the two. The differences between the configurations calibrated over 2017 or 2018 are significant. This points out a lack of robustness for such short calibration periods. Further steps are needed to determine a more reliable implementation.

The outliers in the RVB figure belong to the MOU zone. This is probably relied with the maximal capacity of 0.15 $m^3 s^{-1}$ for the intake of Mourti which induced larger errors when comparing observed and modeled data.

The validation with MODIS data shows that the two models "calibrated" and RAD tend to underestimate the snow covered area, whereas the assimilated models tend to an overestimation. This supports the hypothesis of snow underestimation by non-assimilated models and snow overestimation by the assimilation of SWE derived from Sentinel-1 data.

In Figure 14 the RAD model shows several areas without snow in the upper region of the catchment (BRA and BEI zones). In the BRA zone, we find a DDF of $S = 12.3\, mm\,^{\circ}C^{-1}d^{-1}$ for the GSM model and in the BEI zone $CFMax = 19.5\, mm\,^{\circ}C^{-1}d^{-1}$ for the HBV model, automatically found during its calibration. These two DDFs are higher than in other zones. In Pellicciotti et al. (2005), they calibrated an optimum DDF for the simple temperature-index models of $7.68\, mm\,^{\circ}C^{-1}d^{-1}$ for snow on the glacier of Arolla in summer 2001. This value is clearly lower than the two DDF mentioned above. This comparison is of course not exact, because other general conditions were given for the modelling. However, this shows the limit of an automatic calibration. For real-time application, the melting factors of BRA and BEI could be manually adjusted.

It has to be mentioned that the conversion of Sentinel-1 derived snow depths to SWE is an element of uncertainty. A source of uncertainties are also the flow observations of Bramois, especially for low discharges. The realization of new salt gauging to improve the rating curve is a necessary prerequisite to any further analysis. Another limiting factor is

the relatively short data series of Sentinel-1. This led to short calibration and validation periods. The availability of new data in the future will help improve the data situation.

For alpine catchments, losses through snow sublimation can play an important role as a non-negligible part of the snowpack will not contribute to melt [see for example Strasser et al. (2008)]. This term is not considered in the presented snow models. As a result, this could contribute to the overestimation of water volumes by Sentinel-1 derived data since in reality, not the entire assimilated snowpack would result in meltwater.

5. Conclusions and Outlook

This project provides insights on potential advantages and disadvantages when using Sentinel-1 derived snow depths for data assimilation. The snow depth data were validated in Chapter 2 against in situ measurements in the region of the Borgne catchment (Canton of Valais, CH). This showed on one hand an acceptable reproduction of the dynamics during the snow accumulation until the peak of accumulation. On the other hand, large differences occurred for some stations.

The calibration of the operational MINERVE model in Chapter 3 led to an improvement of Nash coefficients for both upper and lower subcatchments. The downside was the underestimation of summer peaks by the calibrated model. A high quality of discharge measurements is essential for a good calibration. However, the station of Bramois showed substantial uncertainties, especially for low discharges. The underlying rating curve must be improved for a further use. Looking at the modelled SWE values, a particular inability of RS MINERVE to model SWE larger than 0.5 m seems to emerge. Further investigations should be carried out to see if this problem is only linked to precipitation underestimations at high altitude.

Two proposed model improvements were tested in Chapter 4: the integration of solar radiation and the assimilation of SWE derived from Sentinel-1. The first showed a promising increase of performance especially for high elevation catchments. The assimilation of SWE data led to contrasting results with an improvement of some indicators but a worsening of others. Furthermore, the differences between the configuration DA17 and DA18 indicate that the methodology is not robust enough. However, the encouraging results in some of the zones demonstrate that this approach should be investigated further. Some ideas to improve the results are presented hereafter.

Apparently, the assimilation of SWE values derived from Sentinel-1 data led to an overestimation of modelled water volumes. This could be due to the fact, that the scaling factor for Sentinel-1 snow depths was calibrated with measuring stations from the whole Northern Hemisphere [Lievens et al. (2019)]. One option would be to recalibrate this factor to get more accurate product over the Alps or to directly scale the Sentinel-1 derived snow depth values using local observations. The integration of longer time series would allow calibration and validation over longer periods in the future. This would very likely lead to more reliable results. Finally, the evolution of the algorithms by Lievens's team should be kept in sight. If one succeeds to correct the errors induces by wet snow conditions in spring, assimilations later in the year would become feasible.

At the same time, there are other possibilities to assimilate Sentinel-1 data for model improvements. In this project, a simple method was chosen, since the SWE values were directly replaced on individual dates. A softer intervention could be done by calibrating some of the model parameters on the basis of SWE series derived from Senitnel-1. This could be interesting for parameters of the virtual weather stations such as the precipita-

tion and temperature gradients or precipitation and temperature correction coefficients. Finally, the integration of snow (and ice) sublimation could decrease the modelled volume error.

In all calibrations done within this project, the resulting parameters tend to cut off summer peaks. At the same time, some configurations probably converged to a local maximum. Other calibration strategies could be chosen in the hope that they might overcome these difficulties:

- Adjusting the range limits of certain important parameters before or after the calibration (manual adjustments).
- Calibration over longer time periods when more data is available. This would surely help to improve the robustness of the model.
- A further division of parameters into more calibration rounds. This might not prevent the flattening of the peaks but would surely reduce convergence to local maxima.
- Finally, to guarantee a better simulation of peak flows, other performance indicators could be tested. In RS MINERVE, for example, the Normalized Peak Error (NPE) was implemented exactly for this reason. However, the downside of this indicator is that only the absolute maximum peaks are considered over the whole time period. It is therefore not appropriate for long calibration periods.

This work is a first promising attempt of integrating Sentinel-1 derived snow depths data to the MINERVE flood forecast system. Even though there are still some challenges to face, the use of remotely sensed snow data to model natural processes could become an important foundation to overcome data scarcity at high altitudes.

References

Adams, T. E., & Pagano, T. C. (2016). Flood Forecasting: A Global Perspective. In T. E. Adams & T. C. Pagano (Eds.), *Flood Forecasting* (pp. xxiii–xlix). Boston: Academic Press. Retrieved from https://www.sciencedirect.com/science/article/pii/B9780128018842099990 doi: 10.1016/B978-0-12-801884-2.09999-0

Andres, N., Badoux, A., Techel, F., & Hegg, C. (2017). *Todesfälle durch Naturgefahrenprozesse in der Schweiz von 1946 bis 2015. Wasser Energie Luft, 109. Jahrgang (Heft 2), 2017.*

Arnold, N. S., Willis, I. C., Sharp, M. J., Richards, K. S., & Lawson, W. J. (1996). A distributed surface energy-balance model for a small valley glacier. I. Development and testing for Haut Glacier d' Arolla, Valais, Switzerland. *Journal of Glaciology*, *42*(140), 77–89. Retrieved 2021-02-26, from https://www.cambridge.org/core/journals/journal-of-glaciology/article/div-classtitlea-distributed-surface-energy-balance-model-for-a-small-valley-glacier-i-development-and-testing-for-haut-glacier-d-arolla-valais-switzerlanddiv/FA6111D701516D3026AFA7E4EFB51604 doi: 10.3189/S0022143000030549

Avanzi, F., Ercolani, G., Gabellani, S., Cremonese, E., Pogliotti, P., Filippa, G., ... Juglair, S. (2020, November). Learning about precipitation orographic enhancement from snow-course data improves water-balance modeling. *Hydrology and Earth System Sciences Discussions*, 1–37. Retrieved 2021-02-24, from https://hess.copernicus.org/preprints/hess-2020-571/ doi: https://doi.org/10.5194/hess-2020-571

Baba, M. W., Gascoin, S., & Hanich, L. (2018, December). Assimilation of Sentinel-2 Data into a Snowpack Model in the High Atlas of Morocco. *Remote Sensing*, *10*(12), 1982. Retrieved 2020-10-06, from https://www.mdpi.com/2072-4292/10/12/1982 doi: 10.3390/rs10121982

Barnett, T. P., Adam, J. C., & Lettenmaier, D. P. (2005, November). Potential impacts of a warming climate on water availability in snow-dominated regions. *Nature*, *438*(7066), 303–309. Retrieved 2021-02-27, from https://www.nature.com/articles/nature04141 doi: 10.1038/nature04141

Bergström, S. (1976). *Development and application of a conceptual runoff model for Scandinavian catchments* (Ph.D. Thesis). Norrköping.

Bergström, S. (1992). *The HBV model – its structure and applications* (No. 4). Norrköping.

Bosello, F., Iglesias, A., Termansen, M., Jeuken, A., Winsemius, H., De Cian, E., ... Garrote, L. (2018). Economy-Wide Impacts of Climate Mitigation and Adaptation Strategies Across European Regions. In *Adapting to Climate Change in Europe* (pp. 245–271). Elsevier. Retrieved 2021-02-27, from https://linkinghub.elsevier.com/retrieve/pii/B9780128498873000058 doi: 10.1016/B978-0-12-849887-3.00005-8

Braithwaite, R. J., & Olesen, O. [U+FFFD] (1990). A Simple Energy-Balance Model to Calculate Ice Ablation at the Margin of the Greenland Ice Sheet. *Journal of Glaciology*, *36*(123), 222–228. Retrieved 2021-02-26, from https://www.cambridge.org/core/journals/journal-of-glaciology/article/simple-energybalance-model-to-calculate-ice-ablation-at-the-margin-of-the-greenland-ice-sheet/CD655B658A0E373FCE116D0FD8D62216 doi: 10.3189/S0022143000009473

Brock, B. W., Willis, I. C., & Sharp, M. J. (2000). Measurement and parameterization of albedo variations at Haut Glacier d'Arolla, Switzerland. *Journal of Glaciology*, *46*(155), 675–688. doi: 10.3189/172756500781832675

CantonValais. (2006). *Plan sectoriel 3ème correction du Rhône* (Tech. Rep.). Valais Switzerland.

Comola, F., Schaefli, B., Ronco, P. D., Botter, G., Bavay, M., Rinaldo, A., & Lehning, M. (2015). Scale-dependent effects of solar radiation patterns on the snow-dominated hydrologic response. *Geophysical Research Letters*, *42*(10), 3895–3902. Retrieved 2021-01-26, from https://agupubs.onlinelibrary.wiley.com/doi/abs/10.1002/2015GL064075 doi: https://doi.org/10.1002/2015GL064075

Duan, Q., Gupta, V. K., & Sorooshian, S. (1993, March). Shuffled complex evolution approach for effective and efficient global minimization. *Journal of Optimization Theory and Applications*, *76*(3), 501–521. Retrieved 2021-02-25, from https://arizona.pure.elsevier.com/en/publications/shuffled-complex-evolution-approach-for-effective-and-efficient-g doi: 10.1007/BF00939380

Duan, Q., Sorooshian, S., & Gupta, V. (1992). Effective and efficient global optimization for conceptual rainfall-runoff models. *Water Resources Research*, *28*(4), 1015–1031. Retrieved from https://agupubs.onlinelibrary.wiley.com/doi/abs/10.1029/91WR02985 doi: https://doi.org/10.1029/91WR02985

Foehn, A. (2019). Radar-rain gauge merging and discharge data assimilation for flood forecasting in Alpine catchments. , 214. Retrieved from http://infoscience.epfl.ch/record/273163 doi: 10.5075/epfl-thesis-9777

Foehn, A., García Hernández, J., Roquier, B., Fluixá-Sanmartín, J., Paredes Arquiola, J., & De Cesare, G. (2019). RS MINERVE – User manual v2.13. (Ed. CREALP, Switzerland)

Foehn, A., García Hernández, J., Schaefli, B., & De Cesare, G. (2018). Spatial interpolation of precipitation from multiple rain gauge networks and weather radar data for operational applications in Alpine catchments. *Journal of Hydrology*, *563*, 1092–1110. Retrieved from http://infoscience.epfl.ch/record/256102 doi: 10.1016/j.jhydrol.2018.05.027

Foehn, A., Schwob, A., Pasetto, D., Hernández, J. G., & De Cesare, G. (2020). Application of an Ensemble Kalman Filter to A Semi-distributed Hydrological Flood Forecasting System in Alpine Catchments. In *Advances in Hydroinformatics* (pp. 319–334). Springer.

García Hernández, J. (2011). Flood management in a complex river basin with a real-time decision support system based on hydrological forecasts. Retrieved from `http://infoscience.epfl.ch/record/172964`

García Hernández, J., Claude, A., Paredes Arquiola, J., Roquier, B., & Boillat, J.-L. (2014). Integrated flood forecasting and management system in a complex catchment area in the Alps—implementation of the MINERVE project in the Canton of Valais. *River Flow 2014, Special Session on Swiss Competences in River Engineering and Restoration*, 87–97. Retrieved from `http://infoscience.epfl.ch/record/202035` doi: 10.1201/b17134-12

García Hernández, J., Foehn, A., Fluixá-Sanmartín, J., Roquier, B., Tristan, B., Paredes Arquiola, J., & De Cesare, G. (2020). RS MINERVE – Technical manual v2.25. (Ed. CREALP, Switzerland)

GrandeDixenceSA. (2015). *Documentation Technique* (Tech. Rep.). Sion. Retrieved 2021-02-24, from `www.grande-dixence.ch`

GrandeDixenceSA. (2020). *Essencedesign.* Retrieved 2021-02-24, from `http://www.GrandeDixence.ch/,http://www.grande-dixence.ch/de`

Greuell, W., & Smeets, P. (2001). Variations with elevation in the surface energy balance on the Pasterze (Austria). *Journal of Geophysical Research: Atmospheres*, *106*(D23), 31717–31727. Retrieved 2021-02-26, from `https://agupubs.onlinelibrary.wiley.com/doi/abs/10.1029/2001JD900127` doi: https://doi.org/10.1029/2001JD900127

Gugerli, R., Gabella, M., Huss, M., & Salzmann, N. (2020, December). Can Weather Radars Be Used to Estimate Snow Accumulation on Alpine Glaciers? An Evaluation Based on Glaciological Surveys. *Journal of Hydrometeorology*, *21*(12), 2943–2962. Retrieved 2021-02-25, from `https://journals.ametsoc.org/view/journals/hydr/aop/JHM-D-20-0112.1/JHM-D-20-0112.1.xml` doi: 10.1175/JHM-D-20-0112.1

Gupta, H. V., Kling, H., Yilmaz, K. K., & Martinez, G. F. (2009, October). Decomposition of the mean squared error and NSE performance criteria: Implications for improving hydrological modelling. *Journal of Hydrology*, *377*(1-2), 80–91. Retrieved 2019-05-21, from `https://linkinghub.elsevier.com/retrieve/pii/S0022169409004843` doi: 10.1016/j.jhydrol.2009.08.003

Hall, D. K., Riggs, G. A., Salomonson, V. V., DiGirolamo, N. E., & Bayr, K. J. (2002, November). MODIS snow-cover products. *Remote Sensing of Environment*, *83*(1-2), 181–194. Retrieved 2021-03-05, from `https://linkinghub.elsevier.com/retrieve/pii/S0034425702000950` doi: 10.1016/S0034-4257(02)00095-0

Hall, D. K., Riggs G., A., Solomonson, V., & SIPS, N. M. (2015a). *MODIS/Aqua Snow Cover Daily L3 Global 500m SIN Grid.* NASA National Snow and Ice Data Center DAAC. Retrieved 2021-03-05, from http://nsidc.org/data/MYD10A1/versions/6 (type: dataset) doi: 10.5067/MODIS/MYD10A1.006

Hall, D. K., Riggs G., A., Solomonson, V., & SIPS, N. M. (2015b). *MODIS/Terra Snow Cover Daily L3 Global 500m SIN Grid.* NASA National Snow and Ice Data Center DAAC. Retrieved 2021-03-06, from http://nsidc.org/data/MOD10A1/versions/6 (type: dataset) doi: 10.5067/MODIS/MOD10A1.006

Jonas, T., Marty, C., & Magnusson, J. (2009, November). Estimating the snow water equivalent from snow depth measurements in the Swiss Alps. *Journal of Hydrology*, *378*(1), 161–167. Retrieved 2020-11-03, from http://www.sciencedirect.com/science/article/pii/S0022169409005848 doi: 10.1016/j.jhydrol.2009.09.021

Jordan, F. (2007). *Modèle de prévision et de gestion des crues-optimisation des opérations des aménagements hydroélectriques à accumulation pour la réduction des débits de crue* (Doctoral dissertation, EPFL-LCH). Retrieved 2015-12-01, from https://infoscience.epfl.ch/record/103727?ln=fr

Kling, H., Fuchs, M., & Paulin, M. (2012, March). Runoff conditions in the upper Danube basin under an ensemble of climate change scenarios. *Journal of Hydrology*, *424-425*, 264–277. Retrieved 2019-05-21, from https://linkinghub.elsevier.com/retrieve/pii/S0022169412000431 doi: 10.1016/j.jhydrol.2012.01.011

Knoben, W. J. M., Freer, J. E., & Woods, R. A. (2019, October). Technical note: Inherent benchmark or not? Comparing Nash–Sutcliffe and Kling–Gupta efficiency scores. *Hydrology and Earth System Sciences*, *23*(10), 4323–4331. Retrieved 2021-02-25, from https://hess.copernicus.org/articles/23/4323/2019/ doi: https://doi.org/10.5194/hess-23-4323-2019

Lievens, H., Demuzere, M., Marshall, H.-P., Reichle, R. H., Brucker, L., Brangers, I., ... De Lannoy, G. J. M. (2019, October). Snow depth variability in the Northern Hemisphere mountains observed from space. *Nature Communications*, *10*(1), 4629. Retrieved 2020-09-28, from https://www.nature.com/articles/s41467-019-12566-y (Number: 1 Publisher: Nature Publishing Group) doi: 10.1038/s41467-019-12566-y

Magnusson, J., Gustafsson, D., Hüsler, F., & Jonas, T. (2014, October). Assimilation of point SWE data into a distributed snow cover model comparing two contrasting methods. *Water Resources Research*, *50*(10), 7816–7835. Retrieved 2015-11-11, from http://doi.wiley.com/10.1002/2014WR015302 doi: 10.1002/2014WR015302

MeteoSwiss. (2020). *Automatic monitoring network - SwissMetNet (SMN).* Retrieved 2021-02-24, from https://www.meteoswiss.admin.ch/home/measurement-and-forecasting-systems/land-based-stations/automatisches-messnetz.html

Nash, J. E., & Sutcliffe, J. V. (1970). River flow forecasting through conceptual models part I — A discussion of principles. *Journal of Hydrology*, *10*(3),

282–290. Retrieved from https://www.sciencedirect.com/science/article/pii/0022169470902556 doi: https://doi.org/10.1016/0022-1694(70)90255-6

Parajka, J., & Blöschl, G. (2008, September). The value of MODIS snow cover data in validating and calibrating conceptual hydrologic models. *Journal of Hydrology*, *358*(3-4), 240–258. Retrieved 2021-03-04, from https://linkinghub.elsevier.com/retrieve/pii/S0022169408002862 doi: 10.1016/j.jhydrol.2008.06.006

Pellicciotti, F., Brock, B., Strasser, U., Burlando, P., Funk, M., & Corripio, J. (2005). An enhanced temperature-index glacier melt model including the shortwave radiation balance: development and testing for Haut Glacier d'Arolla, Switzerland. *Journal of Glaciology*, *51*(175), 573–587. Retrieved 2021-01-20, from https://www.cambridge.org/core/journals/journal-of-glaciology/article/an-enhanced-temperatureindex-glacier-melt-model-including-the-shortwave-radiation-balance-development-and-testing-for-haut-glacier-darolla-switzerland/E96A8B8D2903523DE6DBF88E2E06E6D9 doi: 10.3189/172756505781829124

Reist, T., & Weingartner, R. (2005). *in Hydrologie der Schweiz – Ausgewählte Aspekte und Resultate. Berichte des BWG, Serie Wasser Nr. 7, Bern.* Retrieved 2021-02-25, from https://scnat.ch/en/id/6kafu

Schaefli, B., Hingray, B., Niggli, M., & Musy, A. (2005). A conceptual glacio-hydrological model for high mountainous catchments. *Hydrology and Earth System Sciences*, *9*(1/2), 95–109. Retrieved from https://hess.copernicus.org/articles/9/95/2005/ doi: 10.5194/hess-9-95-2005

Shepard, D. (1968). A two-dimensional interpolation function for irregularly-spaced data. In *Proceedings of the 1968 23rd ACM national conference on* - (pp. 517–524). ACM Press. Retrieved 2021-02-11, from http://portal.acm.org/citation.cfm?doid=800186.810616 doi: 10.1145/800186.810616

Shiklomanov, I. A. (1993). *World freshwater resources. Water in crisis: a guide to the world's fresh water resources.* Oxford University Press, New York.

Sideris, I. V., Gabella, M., Erdin, R., & Germann, U. (2014, April). Real-time radar-rain-gauge merging using spatio-temporal co-kriging with external drift in the alpine terrain of Switzerland: Real-time radar-rain-gauge merging. *Quarterly Journal of the Royal Meteorological Society*, *140*(680), 1097–1111. Retrieved 2021-03-07, from http://doi.wiley.com/10.1002/qj.2188 doi: 10.1002/qj.2188

Slater, A. G., & Clark, M. P. (2006, June). Snow Data Assimilation via an Ensemble Kalman Filter. *Journal of Hydrometeorology*, *7*(3), 478–493. Retrieved 2015-11-12, from http://journals.ametsoc.org/doi/abs/10.1175/JHM505.1 doi: 10.1175/JHM505.1

SLF. (2020). *IntercantonalMeasurement and Information System (IMIS). WSL Institute for Snow and Avalanche Research SLF.* Retrieved 2020-10-24, from https://www.slf.ch/de/lawinenbulletin-und-schneesituation/messwerte/beschreibung-automatische-stationen.html

Strasser, U., Bernhardt, M., Weber, M., Liston, G. E., & Mauser, W. (2008). Is snow sublimation important in the alpine water balance? *The Cryosphere*, *2*(1), 53–66. Retrieved from https://tc.copernicus.org/articles/2/53/2008/ doi: 10.5194/tc-2-53-2008

Vögeli, C., Lehning, M., Wever, N., & Bavay, M. (2016). Scaling Precipitation Input to Spatially Distributed Hydrological Models by Measured Snow Distribution. *Frontiers in Earth Science*, *4*. Retrieved 2021-02-01, from https://www.frontiersin.org/articles/10.3389/feart.2016.00108/full doi: 10.3389/feart.2016.00108

Willis, I. C., Arnold, N. S., & Brock, B. W. (2002). Effect of snowpack removal on energy balance, melt and runoff in a small supraglacial catchment. *Hydrological Processes*, *16*(14), 2721–2749. Retrieved 2021-02-26, from https://onlinelibrary.wiley.com/doi/abs/10.1002/hyp.1067 doi: https://doi.org/10.1002/hyp.1067

Appendices

A.

A.1. SWE comparison

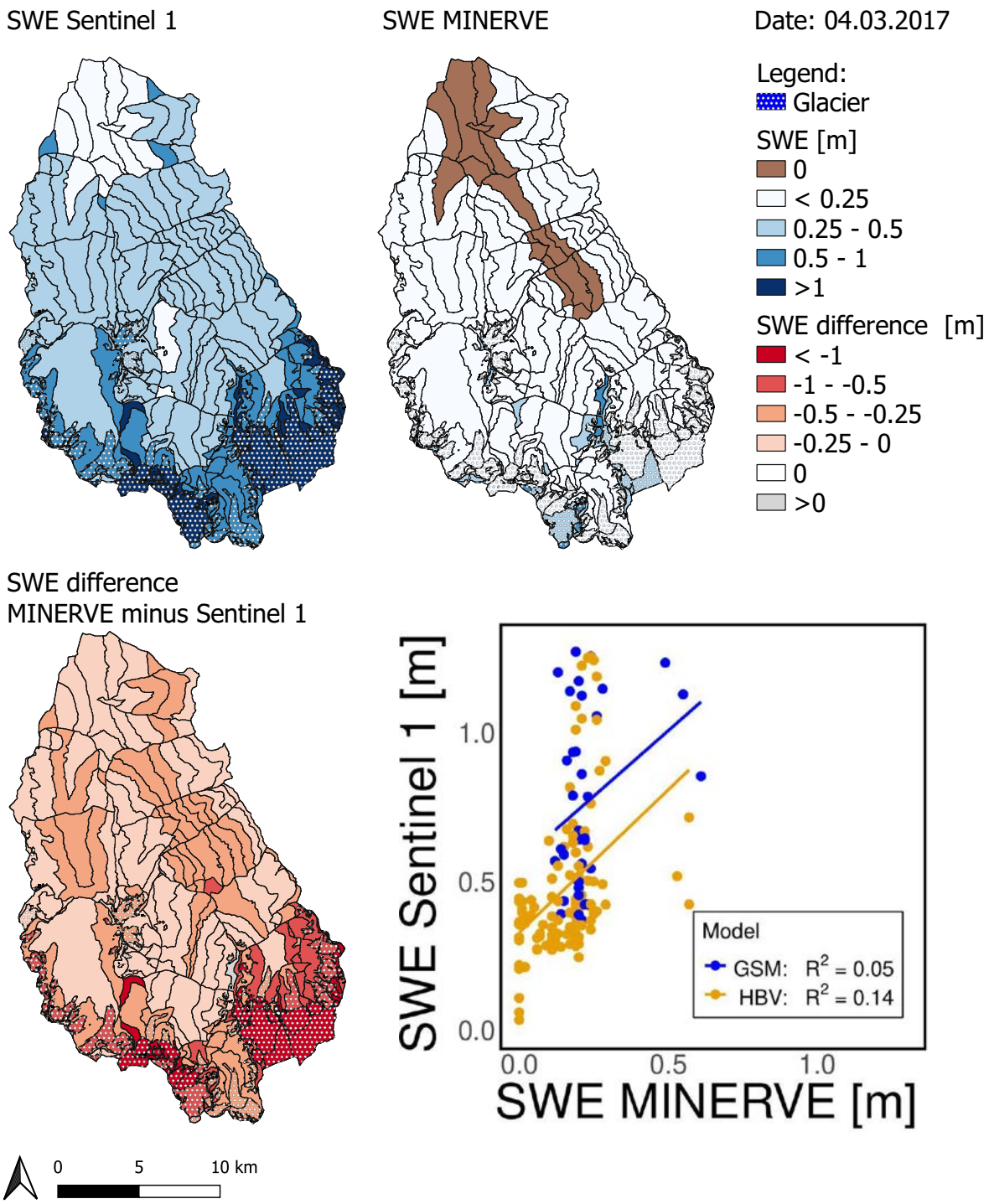

Figure 16: Comparison of modelled snow water equivalent (SWE) with SWE derived from Sentinel 1 snow data for the 4th of March 2017. The upper plots show the absolute SWE values for both Sentinel 1 (top left) and the calibrated MINERVE model (top right). The difference of the two is shown on the bottom left (MINERVE minus Sentinel 1). The scatter plot on the bottom right shows MINERVE and Sentinel 1 derived SWE grouped by the two models (GSM and HBV).

A.2. Sensitivity analysis

Table 8: Initial an calibrated parameters of the BRI catchment.

Nr.	Parameter	Unit	initial value	calibrated value	under limit	upper limit
1	S	[mm/C°/d]	5	5.31	0.5	20
2	G	[mm/C°/d]	5	4.88	0.5	20
3	Kgl	[dˆ-1]	4.5	0.58	0.1	5
4	Ksn	[dˆ-1]	4.5	1.49	0.1	5
5	CFMax	[mm/C°/d]	5	9.36	0.5	20
6	Beta	[-]	2.5	1.00	1	5
7	FC	[m]	0.25	0.06	0.05	0.65
8	PWP	[-]	0.5	0.19	0.03	1
9	SUMax	[m]	0.05	0.09	0.001	0.1
10	Kr	[dˆ-1]	0.3	0.21	0.05	0.5
11	Ku	[dˆ-1]	0.1	0.05	0.01	0.4
12	Kl	[dˆ-1]	0.02	0.04	0	0.15
13	Kperc	[dˆ-1]	0.15	0.79	0	0.8

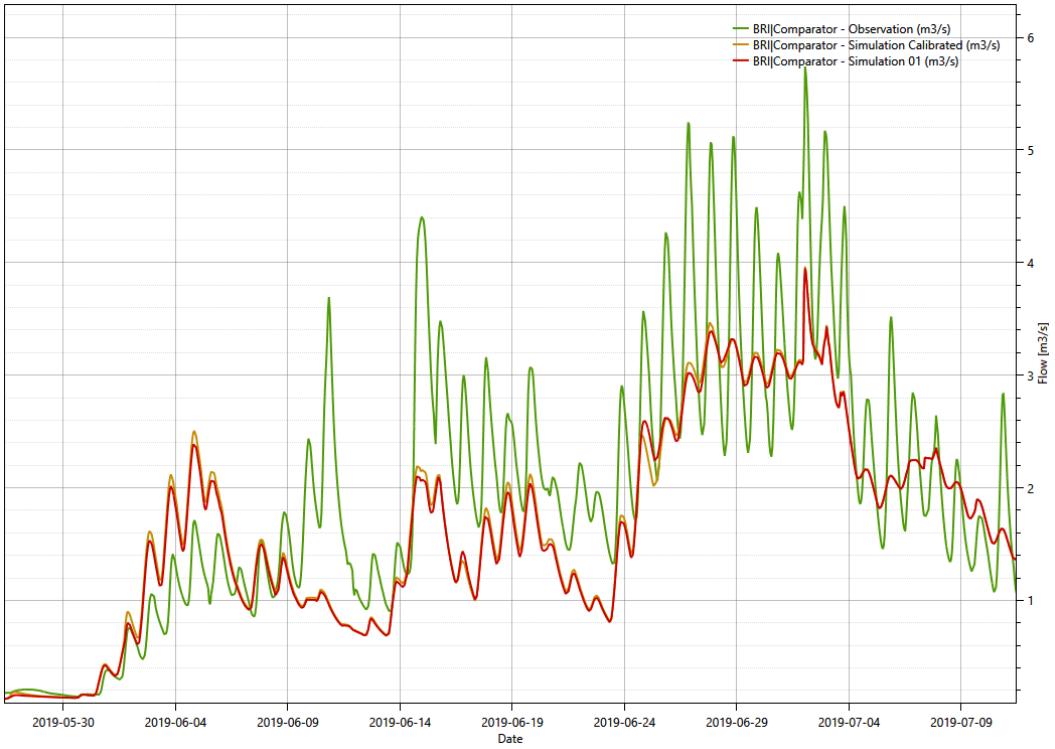

Figure 17: Flow hydrograph of the BRI catchment; measured (green), calibrated (orange) and adjustment of S (GSM) to the initial value (red).

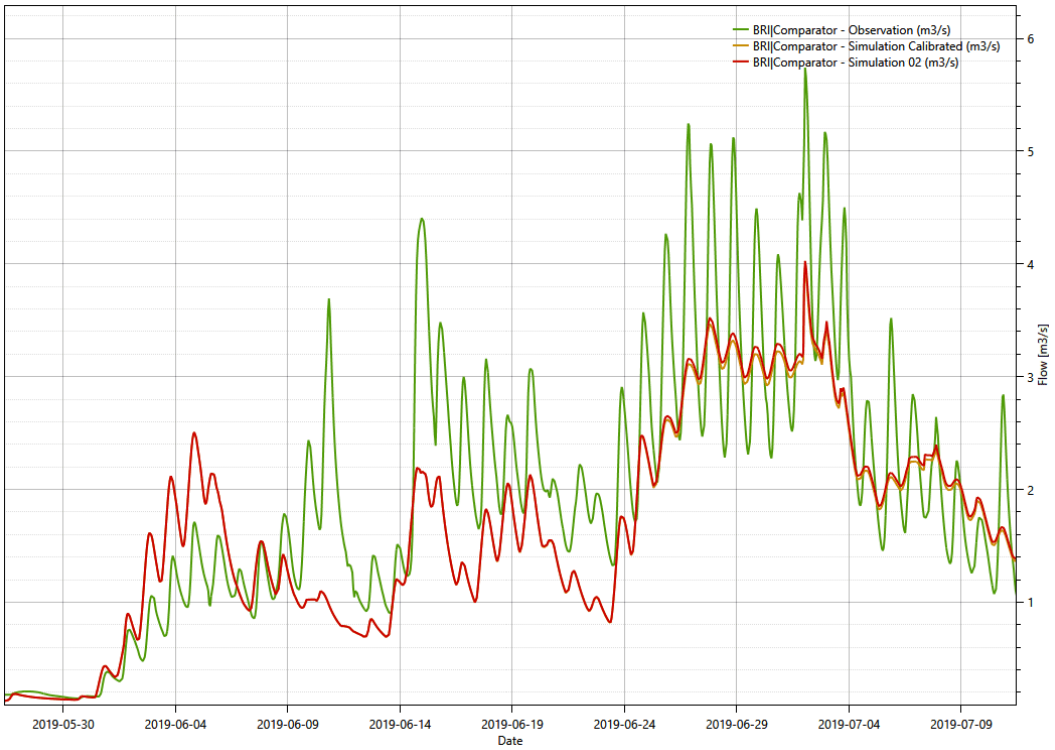

Figure 18: Flow hydrograph of the BRI catchment; measured (green), calibrated (orange) and adjustment of G (GSM) to the initial value (red).

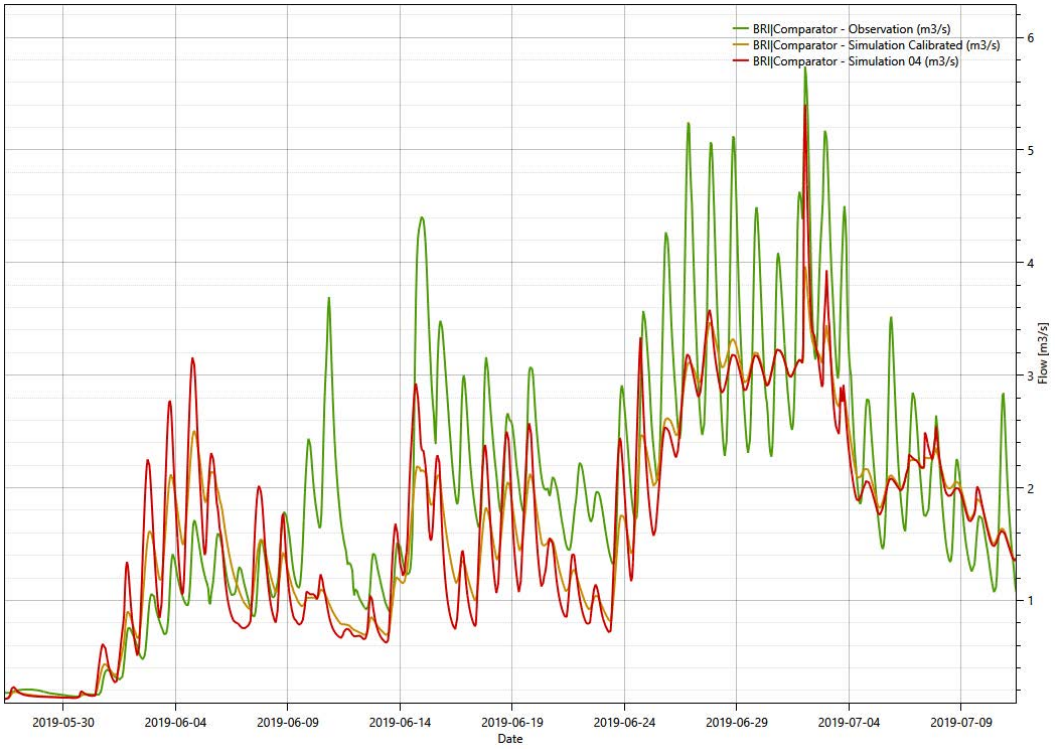

Figure 19: Flow hydrograph of the BRI catchment; measured (green), calibrated (orange) and adjustment of Ksn (GSM) to the initial value (red).

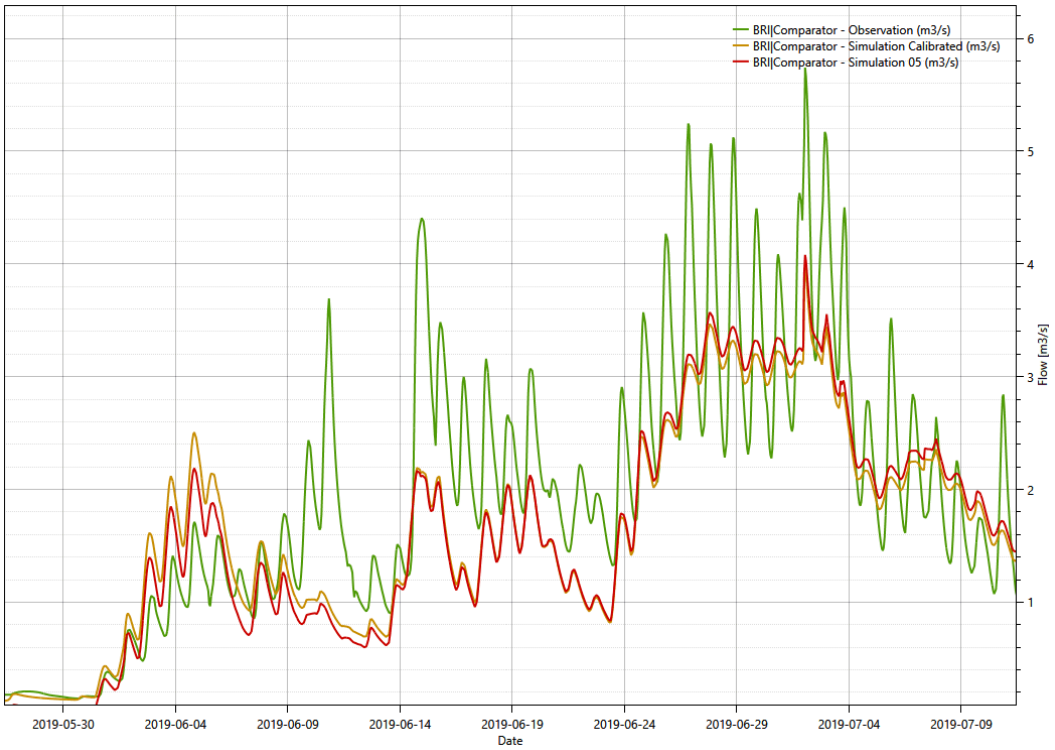

Figure 20: Flow hydrograph of the BRI catchment; measured (green), calibrated (orange) and adjustment of CFMax (HBV) to the initial value (red).

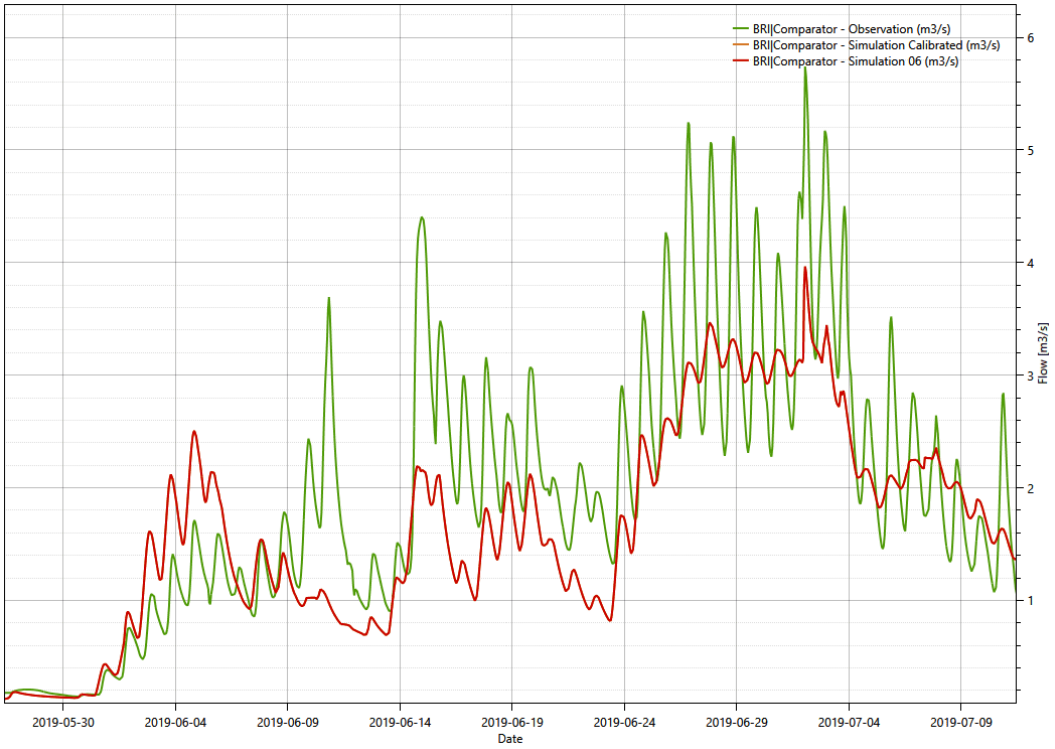

Figure 21: Flow hydrograph of the BRI catchment; measured (green), calibrated (orange) and adjustment of Beta (HBV) to the initial value (red).

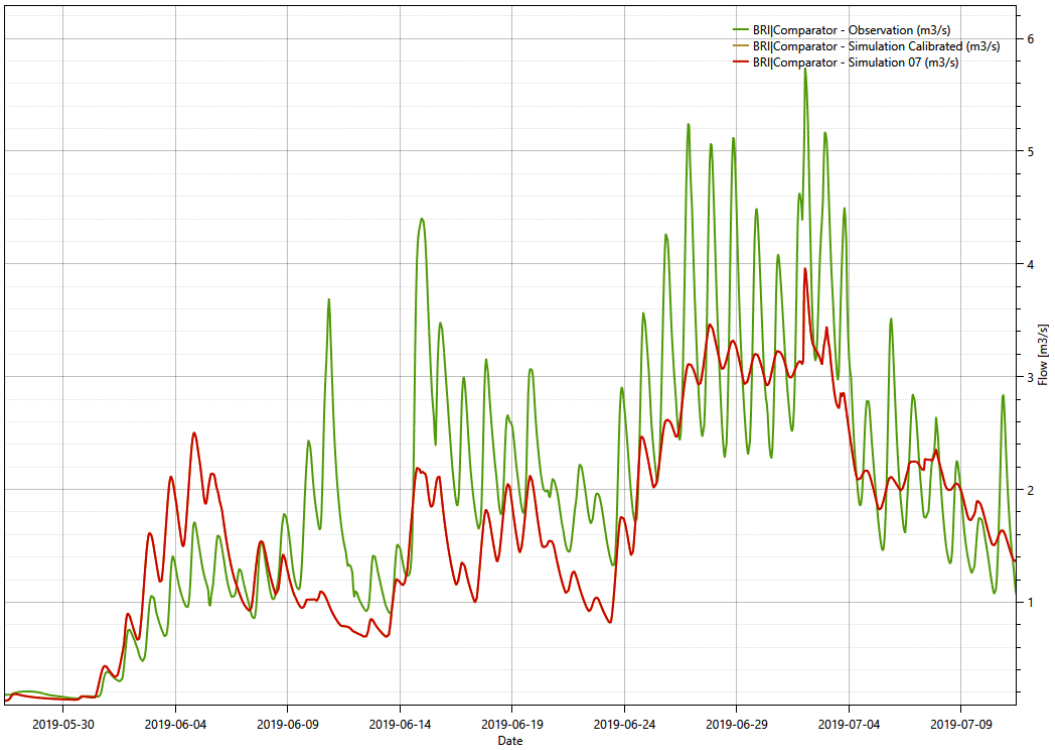

Figure 22: Flow hydrograph of the BRI catchment; measured (green), calibrated (orange) and adjustment of FC (HBV) to the initial value (red).

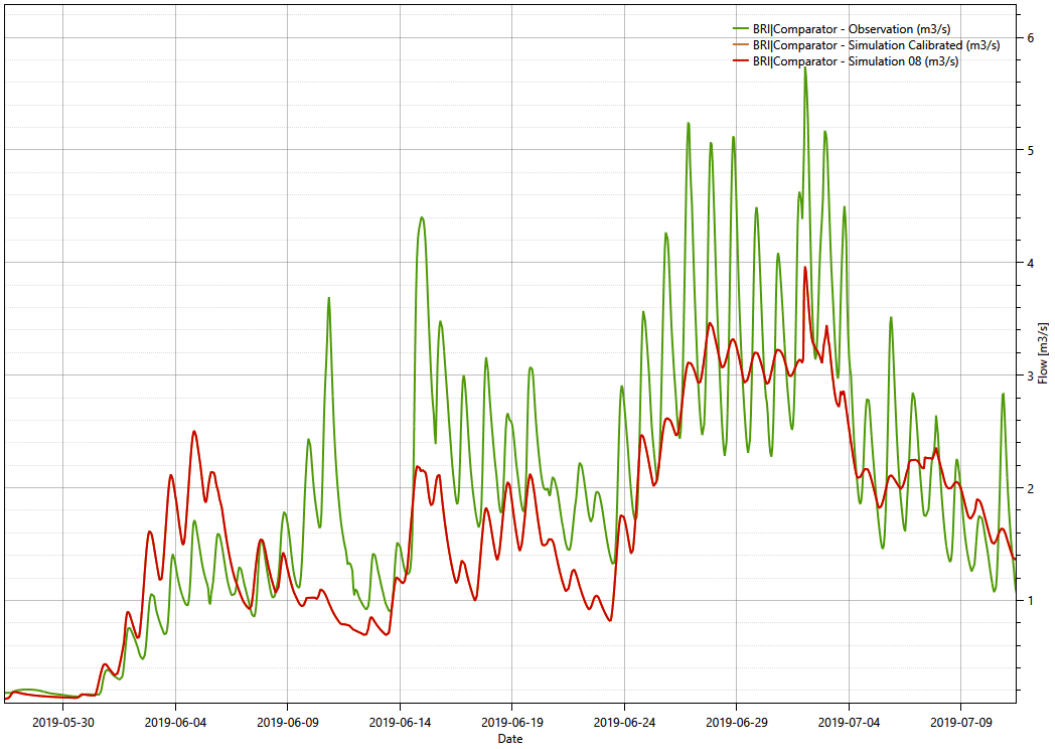

Figure 23: Flow hydrograph of the BRI catchment; measured (green), calibrated (orange) and adjustment of PWP (HBV) to the initial value (red).

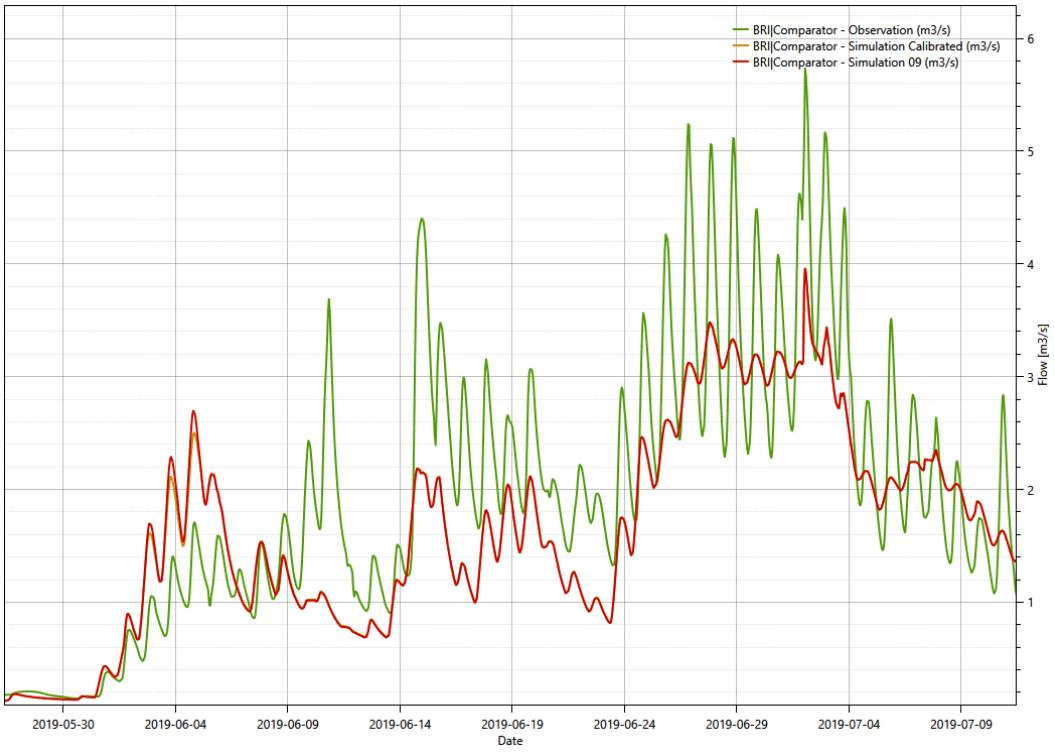

Figure 24: Flow hydrograph of the BRI catchment; measured (green), calibrated (orange) and adjustment of SUMAX (HBV) to the initial value (red).

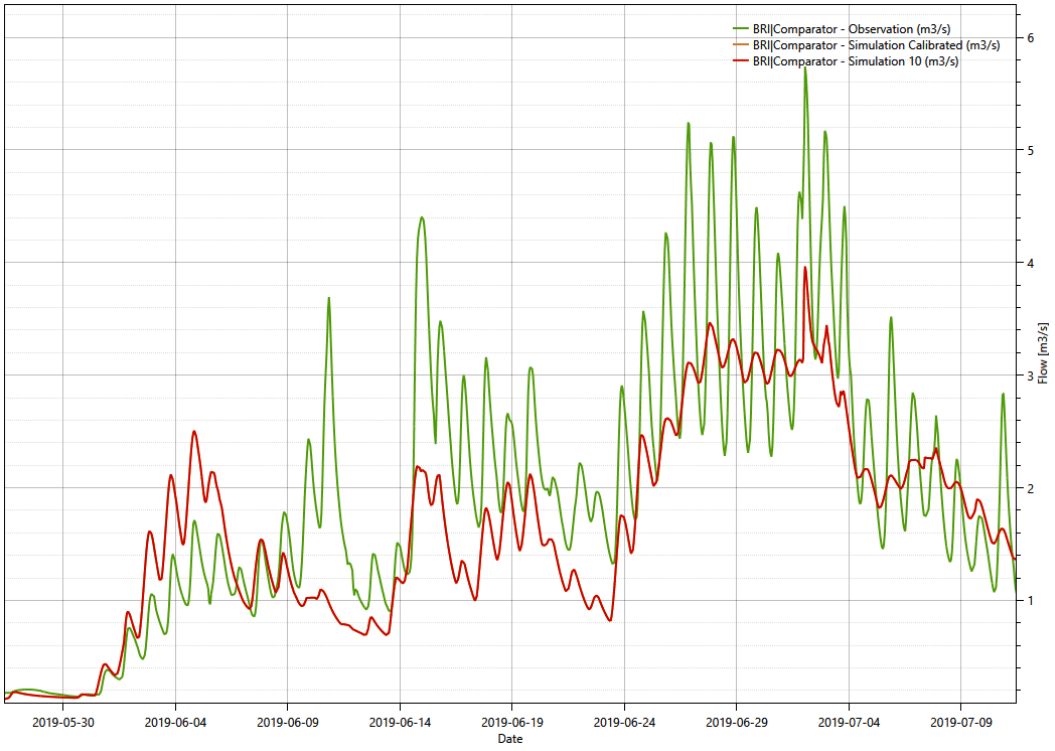

Figure 25: Flow hydrograph of the BRI catchment; measured (green), calibrated (orange) and adjustment of Kr (HBV) to the initial value (red).

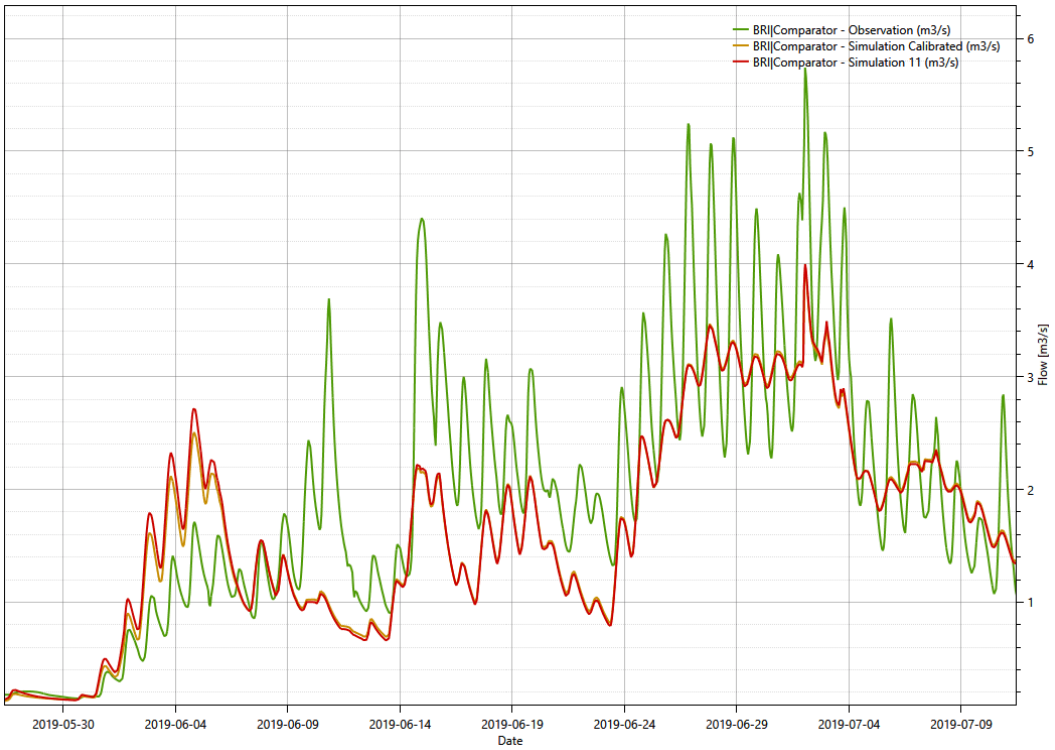

Figure 26: Flow hydrograph of the BRI catchment; measured (green), calibrated (orange) and adjustment of Ku (HBV) to the initial value (red).

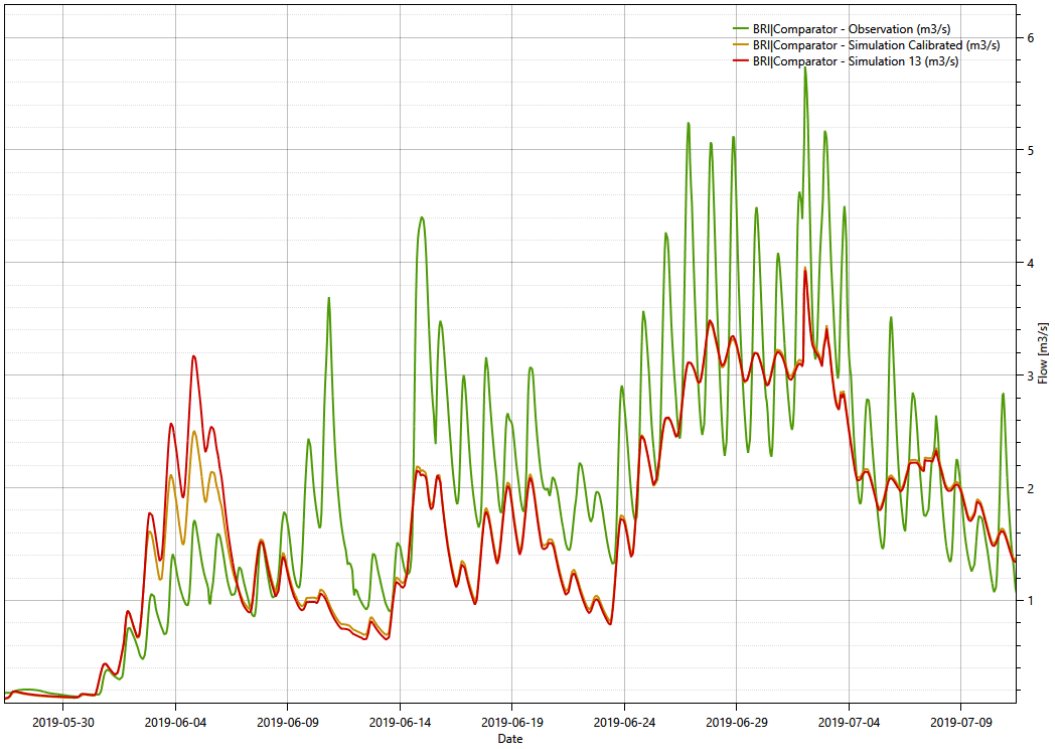

Figure 27: Flow hydrograph of the BRI catchment; measured (green), calibrated (orange) and adjustment of Kperc (HBV) to the initial value (red).

A.3. Nash-ln and KGE

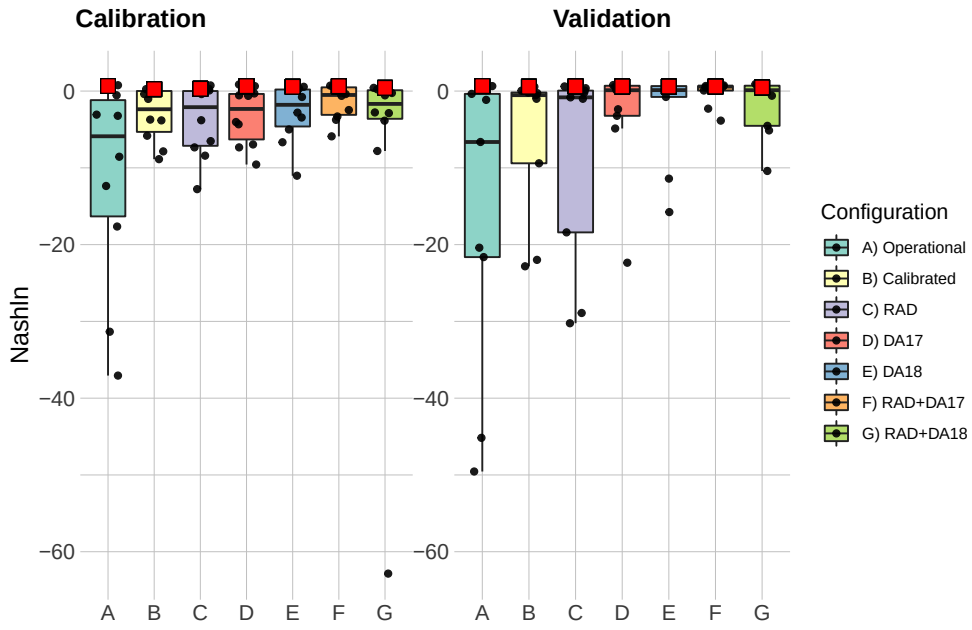

Figure 28: Nash-ln coefficients of the seven model configurations (A-G) for the calibration and the validation periods. The boxplots represent the median (bold horizontal line) and the 25 and 75 quantiles (hinges) for the indicators of the ten calibration zones (without BEI for the validation). The the lower and upper whiskers extend from the hinge to the largest value no further than 1.5 * inter-quartile range from the hinge. The red square indicates the value for the station of Bramois.

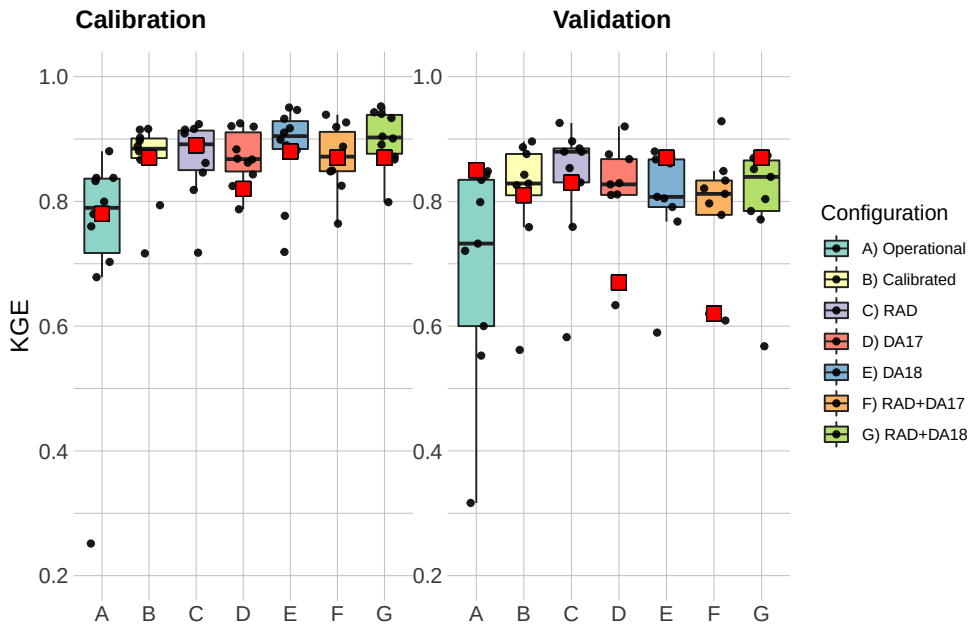

Figure 29: Kling-Gupta efficiencies (KGE) of the seven model configurations (A-G) for the calibration and the validation periods. The boxplots represent the median (bold horizontal line) and the 25 and 75 quantiles (hinges) for the indicators of the ten calibration zones (without BEI for the validation). The the lower and upper whiskers extend from the hinge to the largest value no further than 1.5 * inter-quartile range from the hinge. The red square indicates the value for the station of Bramois.

A.4. Calibrated parameters Bramois

Table 9: Parameters resulting of the calibration of the different configurations for Bramois.

Model	Name	UNIT	Calib	RAD	DA17	DA18	RAD +DA17	RAD +DA18
GSM	S	[mm/C°/d]	17.75	12.29	0.078	9.04	14.96	1.44
	SFR	[mm/W/d]	-	0.71	-	-	0.89	0.18
	G	[mm/C°/d]	7.35	0.55	0.14	0.02	0.01	0.02
	Kgl	[dˆ-1]	5.00	1.12	2.32	3.70	3.29	3.70
	Ksn	[dˆ-1]	5.00	4.22	4.17	3.80	2.42	0.14
	IFR	[mm/W/d]	-	0.53	-	-	0.002	0.001
HBV	CFMax	[mm/C°/d]	2.45	2.65	2.33	2.70	2.11	2.54
	SFR	[mm/W/d]	-	0.002	-	-	0.0003	0.01
	Beta	[-]	1.00	1.00	1.79	1.00	1.00	1.00
	FC	[m]	0.17	0.10	0.23	0.54	0.18	0.57
	PWP	[-]	0.45	0.49	0.98	0.87	0.70	0.28
	SUMax	[m]	0.01	0.03	0.05	0.10	0.04	0.01
	Kr	[dˆ-1]	0.39	0.18	0.35	0.34	0.15	0.50
	Ku	[dˆ-1]	0.02	0.05	0.05	0.04	0.04	0.01
	Kl	[dˆ-1]	0.058	0.058	0.004	0.050	0.003	0.090
	Kperc	[dˆ-1]	0.80	0.27	0.16	0.00004	0.16	0.61

A.5. Performance indicators Bramois

Table 10: Performance indicators Nash Nashln, RVB and KGE for the zone of Bramois for the seven model configurations.

	Calibration				Validation			
Configuration	Nash	Nash-ln	RVB	KGE	Nash	Nash-ln	RVB	KGE
OP	0.56	0.66	-0.04	0.78	0.76	0.65	-0.07	0.85
CALIB	0.79	0.25	-0.09	0.87	0.80	0.57	-0.12	0.81
RAD	0.78	0.30	-0.03	0.89	0.81	0.61	-0.09	0.83
DA17	0.68	0.64	0.07	0.82	0.72	0.60	0.08	0.67
DA18	0.78	0.56	-0.016	0.88	0.79	0.59	0.07	0.87
RAD_DA17	0.75	0.63	-0.019	0.87	0.68	0.59	0.06	0.62
RAD_DA18	0.77	0.42	-0.019	0.87	0.79	0.47	0.07	0.87

A.6. MODIS validation

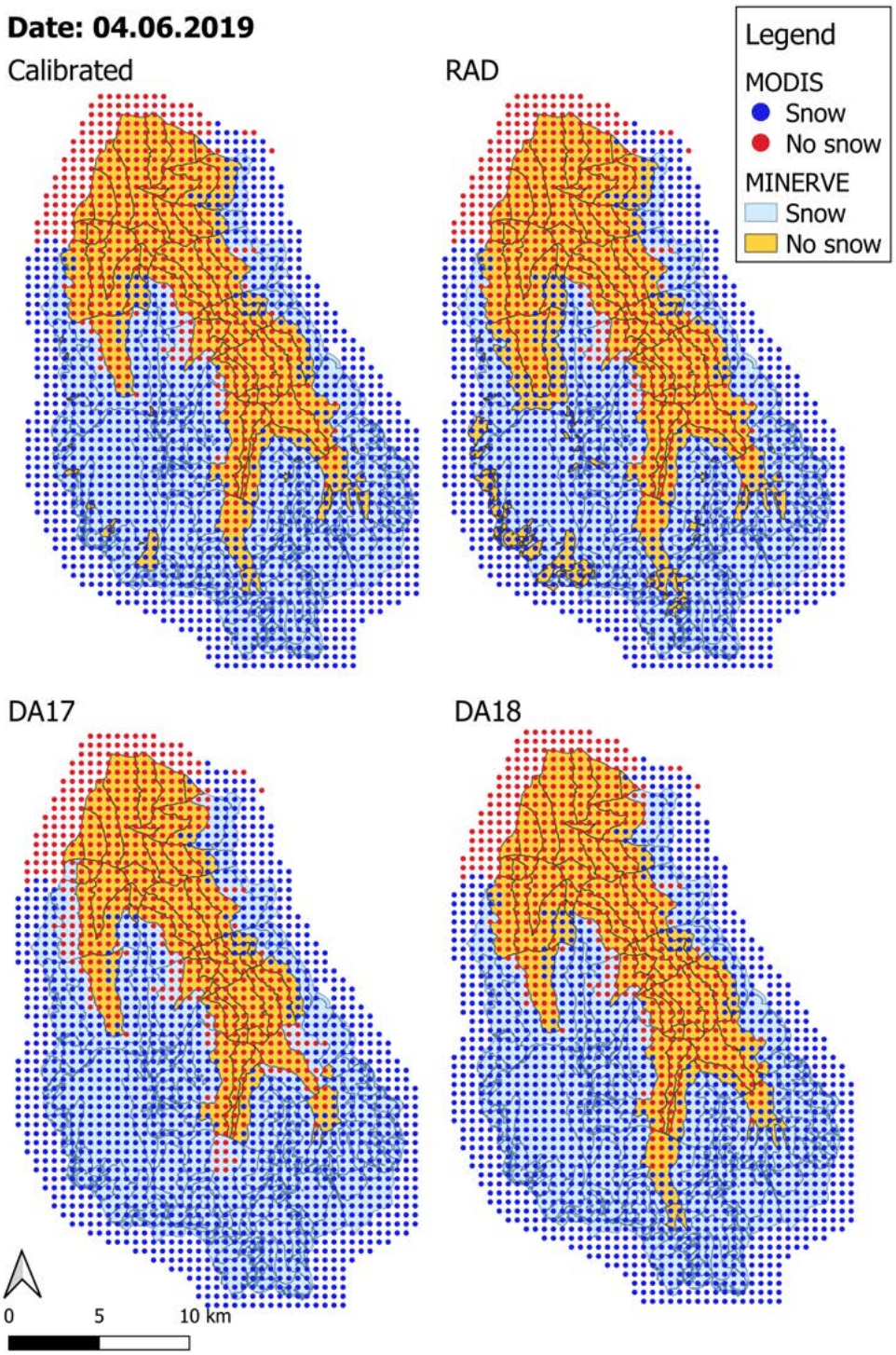

Figure 30: Modeled snow cover of four configurations on the 4th of June 2019 compared to observed snow cover by MODIS.

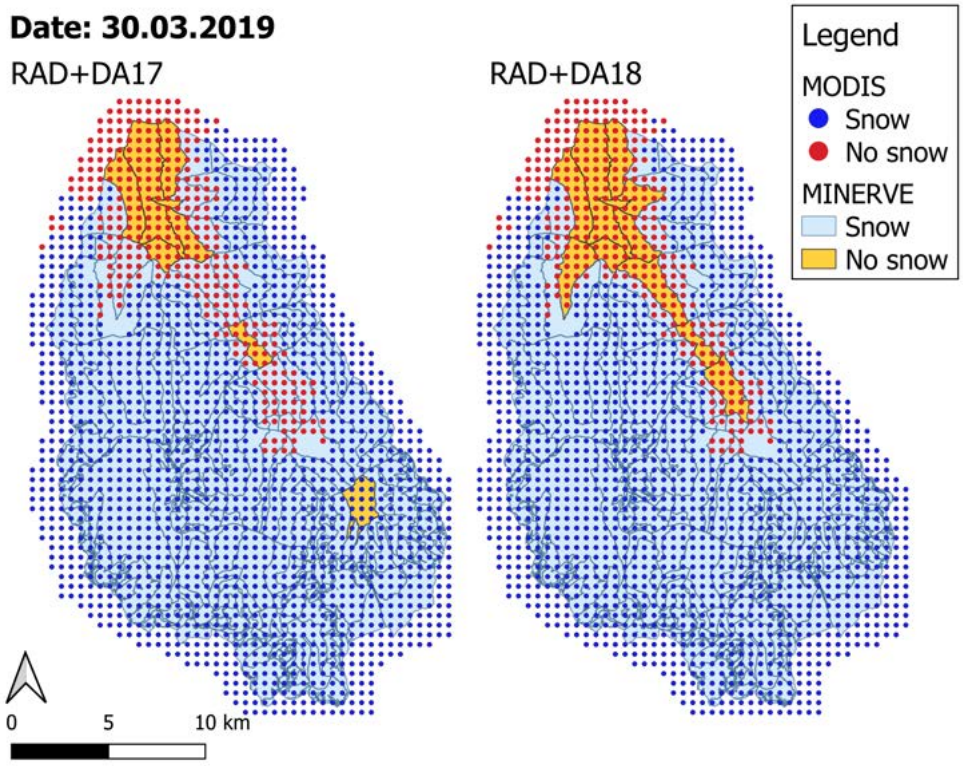

Figure 31: Modeled snow cover of two configurations on the 30th of March 2019 compared to observed snow cover by MODIS.

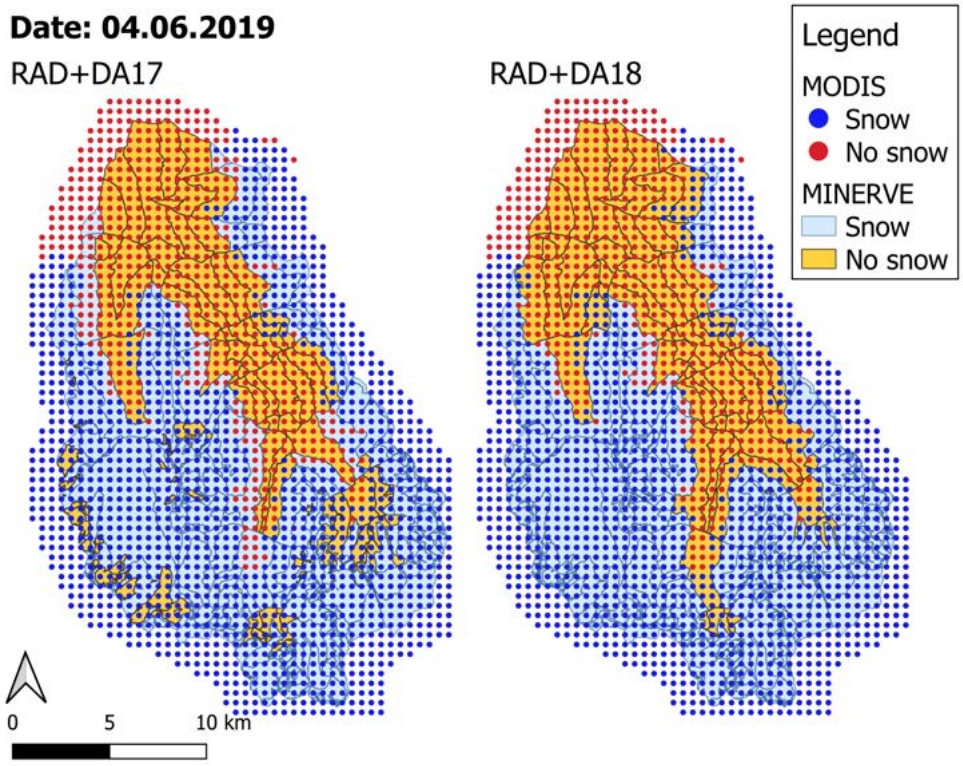

Figure 32: Modeled snow cover of two configurations on the 4th of June 2019 compared to observed snow cover by MODIS.

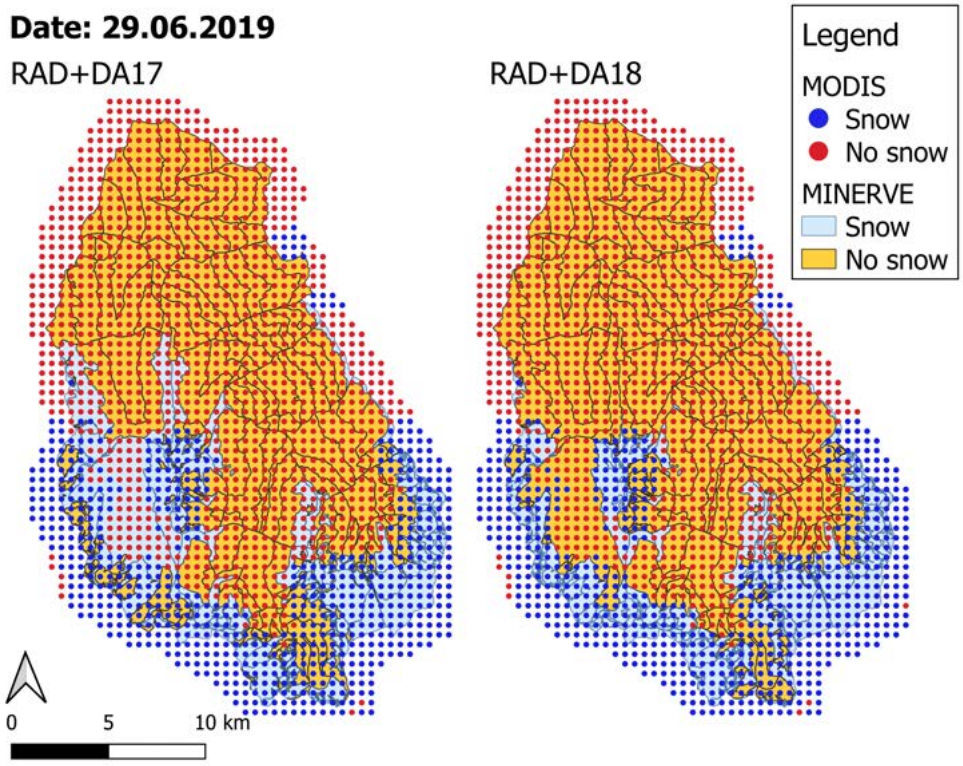

Figure 33: Modeled snow cover of two configurations on the 29th of June 2019 compared to observed snow cover by MODIS.